DTI-based tractographic analysis of white matter alterations in HIV infected children

By Joanah Madzime

MDZJOA001

In fulfilment of the requirements for the degree of Master of Science (Medicine) in Neurosciences.

Faculty of Health Sciences

UNIVERSITY OF CAPE TOWN

February, 2019

Supervisor: Dr. Marcin Jankiewicz

Co-supervisor: Dr. Martha Holmes

Co-supervisor: Prof. Ernesta Meintjes

University of Cape Town

The copyright of this thesis vests in the author. No quotation from it or information derived from it is to be published without full acknowledgement of the source. The thesis is to be used for private study or non-commercial research purposes only.

Published by the University of Cape Town (UCT) in terms of the non-exclusive license granted to UCT by the author.

University of Cape Town

DECLARATION

I, JOANAH MADZIME, hereby declare that the work on which this thesis is based is my own original work (except where acknowledgements indicate otherwise) and that neither the whole, nor any part of it, has been, or is to be submitted for any other degree in this or any other University.

I empower the University to reproduce, for the purpose of research, either the whole or part of the contents of this thesis in any manner.

Signed by candidate

Signature

09 Feb. 19

Date

ACKNOWLEDGEMENT

I would like to start by thanking the Lord, Almighty God for providing me strength, wisdom and sustenance though the completion of this degree; without Him, nothing is possible.

I must express my absolute appreciation to my supervisor, Dr Marcin Jankiewicz for all the expert ideas, resources, guidance, support and encouragement through the duration of this project. I have learnt so much from him and I am grateful.

A big thank you to my co-supervisors, Dr Martha Holmes for the countless hours she sacrificed to help me see this project through as well as Professor Ernesta Meintjes for her guidance and support.

Special thanks to the National Research Foundation (NRF) and National Institutes of Health (NIH) for the financial support which made this project possible.

I would like to appreciate the entire MRI research group, for their support and friendships through the duration of this project.

Finally, I would like to express my gratitude to my family. I appreciate my mother and father for their sacrifices, unconditional love and prayers without which I would not have gotten this far. I am grateful to my sister for all that she is in a best friend and whose humourous nature kept me sane. Thank you to my brother for being a constant source of joy and light. I appreciate Farai Mberi for his constant support and prayers.

ABSTRACT

Despite early combination antiretroviral therapy (cART) administration, children born with human immunodeficiency virus (HIV) continue to demonstrate neurodevelopmental abnormalities. Often, there is a link between structural and functional abnormalities. Previously, we found HIV-associated changes in white matter and functional networks in a cohort of 7-year-old HIV infected (HIV+) children who intiatied early cART compared to uninfected controls. To explore possible relationships between these alterations, we used tractography to identify HIV-related abnormalities within structural connections located in functional resting state networks.

Within HIV+ children (n=61), we identified white matter (WM) tracts with lower mean fractional anisotropy (FA) and/or higher mean diffusivity (MD) located in several functional networks, including the somatosensory, auditory, salience, default mode network (DMN), motor and basal ganglia networks compared to uninfected controls (n=46). Among the uninfected controls, children born to HIV+ mothers (exposed uninfected, HEU) (n=19) showed WM alterations (higher FA) compared to HIV unexposed uninfected children (HUU) (n=27) within tracts in the posterior DMN, visual (occipital lobe and lingual gyrus), salience and motor networks.

The observed WM alterations in HIV+ children point to demyelination/dysmyelination within six networks. Four of these networks – the basal ganglia, default mode, salience and somatosensory – were all found to have altered functional connectivity in a previous study; therefore, these results point to damage or developmental delay in white matter may be related to or responsible for the HIV-associated functional abnormalities. The observed WM alterations in the HEU children suggest that even exposure to HIV and/or antiretroviral therapy (ART) also has long-term effects on axonal integrity in the developing brain.

TABLE OF CONTENTS

LIST OF FIGURES

LIST OF TABLES

LIST OF ABBREVIATIONS

3D	3-dimensional
AD	axonal diffusivity
AFNI	analysis of functional neuroimages
AIDS	acquired immune deficiency virus
ANCOVA	analysis of covariance
AP	Anterior-Posterior
ART	antiretroviral treatment
ART-Def	ART deferred until CD4% < 25% in first year or CD4% < 20% thereafter, or if clinical disease progression criteria presented
ART-40W	ART initiated immediately and interrupted after 40 weeks
ART-96W	ART initiated immediately and interrupted after 96 weeks
ATR	anterior thalamic radiation
BBB	blood brain barrier
BOLD	blood oxygen level dependent
cART	combination antiretroviral therapy
CD	cluster of differentiation
CHER	children with early antiretroviral therapy
CNS	central nervous system
CPE	CNS penetration effectiveness
CSF	cerebrospinal fluid
CST	corticospinal tract
CUBIC	Cape Universities Brain Imaging Center
dATT	dorsal attention
DMN	default mode network
DT	deterministic
DTI	diffusion tensor imaging
DWI	diffusion weighted imaging
FA	fractional anisotropy
FAMCRU	family clinical research unit
FATCAT	functional and tractographic connectivity analysis toolbox
FDR	false discovery rate
FM	forceps minor
fMRI	functional magnetic resonance imaging
GM	grey matter
HAART	highly active antiretroviral therapy
HEU	HIV exposed uninfected
HIV	human immunodeficiency virus
HUU	HIV unexposed uninfected
IFOF	inferior fronto-occipital fasciculus
ILF	inferior longitudinal fasciculus
MD	mean diffusivity
MEMPRAGE	Multi-echo magnetization prepared rapid gradient echo
MINIP	mini-probabilistic
MRS	magnetic resonance spectroscopy
MTCT	mother to child transmission
PA	Posterior-Anterior
pDMN	posterior DMN
PROB	probabilistic
vDMN	ventral DMN

RD	radial diffusivity
RF	radiofrequency
RS-fMRI	resting state-fMRI
RSN	resting state network
SFOF	superior fronto-occipital fasciculus
SLF	superior longitudinal fasciculus
TE	echo time
TORTOISE	Tolerably obsessive registration and tensor optimization indolent software ensemble
TR	repetition time
WM	white matter

1. INTRODUCTION

At the end of 2017, approximately 1.8 million children were living with HIV globally (UNAIDS, 2018). There were at least 180 000 new paediatric HIV infections and over 50% of those reside in east and southern Africa. Treatment accessibility has improved, with about 60% of children living with HIV in east and southern African having access to treatment (UNAIDS, 2018). In South Africa, at least 280 000 children were living with HIV by the end of 2017, which is almost 4% of the total HIV infected population (StatsSA, 2018). According to UNAIDS estimates, of the 15 million HEU children, approximately 20% are living in South Africa, making it the country with the highest HIV statistics worldwide. Among children born to HIV infected mothers, there is a growing population of HEU as well as HIV infected children who are growing up with treatment. The long-term effects of HIV infection and exposure on the developing child in the era of early treatment is not well known.

The virus enters the central nervous system (CNS) soon after infection which may harm the child's developing brain (Ellis et al., 2009). Combination antiretroviral therapy (cART) protects the developing brain from the virus and thus has led to lower mortality rates in children, however it has limited ability to penetrate the blood-brain-barrier (BBB) (Ene et al., 2011). This allows for ongoing replication of the virus in the brain and formation of drug resistant populations. Thus, despite increased access and early initiation of cART in children born to HIV infected mothers, perinatally infected children continue to demonstrate neurologic abnormalities as well as neurocognitive delays and deficits.

In the brain, the virus affects grey matter (GM), the functional part of the brain where signal/information processing takes place, as well as WM, the structural part of the brain that carries electrical signals between GM regions. Anatomically separate GM regions with temporal correlations in neuronal activity patterns form functional networks (identified by resting-state functional magnetic resonance imaging (RS-fMRI)). Due to the interdependence of structure and function in the brain, the HIV virus may affect the development of functional networks by compromising grey and/or white matter. Diffusion tensor imaging (DTI) (O'Donnell & Westin, 2011a) is a technique used to measure microstructural properties of white matter. With these measures, one can map WM tracts, and this is known as DTI tractography. The maps of WM tracts

represent connections between GM regions. Tractography allows one to see if HIV-associated compromises in structural integrity (characterised by low FA and high MD (Tromp, 2016)) may be related to HIV related alterations in functional connectivity.

Multi-modal studies in healthy subjects demonstrate association between functional and structural connectivity (Hagmann et al., 2008; Koch, Norris et al., 2002; Skudlarski et al., 2008; van den Heuvel et al, 2008). For example, FA in the cingulum bundle, which connects different GM regions within the default mode network (DMN), has been shown to be related to temporal correlations of blood oxygen level dependent (BOLD) signals from GM regions connected by this tract (van den Heuvel et al., 2008). The general consensus seems to be that, in the presence of a structural connection, the integrity of this connection reflects the functional connectivity between the connected regions. However, since functionally connected regions may be connected via a third (or a series of intermediate) GM region(s), functional connectivity does not necessarily imply that a direct structural connection exists (Greicius et al., 2009; Honey et al., 2009).

This underlying relationship between structural and functional connectivity is the basis for the current study. Given the dependence between structural and functional connectivity, we decided to investigate possible relationships between HIV-associated functional and structural abnormalities. As part of a longitudinal neurodevelopmental study looking at the impact of HIV, we have identified HIV-associated structural and functional abnormalities in 7-year-old children. Using RS-fMRI, we found significant differences in mean functional connectivity in clusters in several networks in HIV+ children (Toich et al., 2018). Most of the differences identified were between networks, with the exception of one connection within the default mode network (DMN) (Toich et al., 2018). In addition, we found higher functional connectivity related to poorer immune health in infancy within the basal ganglia, somatosensory and salience networks (Toich et al., 2018). Within the same cohort at age 7, we performed a voxelwise DTI study, which revealed numerous regions demonstrating HIV associated abnormalities. In the HIV+ children we reported FA reductions in the left inferior fronto-occipital fasciculus (IFOF) and inferior longitudinal fasciculus (ILF), as well as increased MD in the IFOF, superior corona radiata, anterior thalamic radiation (ATR) and right forceps minor (FM) compared to uninfected children (Jankiewicz et al., 2017). Furthermore, the study showed increased mean FA in the posterior corona radiata as

well as lower mean MD in the corticospinal tract (CST) in HEU compared to HUU children (Jankiewicz et al., 2017).

To explore the possible relationship between the HIV related changes reported in the aforementioned papers, we performed a DTI-based tractography study within the identified resting state networks (RSNs) of our cohort at age 7.

Specifically, we examined the effects of HIV/ART on WM tracts/connections between GM regions within previously identified RSNs. For each WM tract, average measures of WM integrity (i.e. FA, MD, axonal diffusivity (AD) and radial diffusivity (RD)) were extracted and compared between HIV+ children and uninfected controls, and among controls between HEU and HUU.

We hypothesised that:

1) Based on our resting state results at age 7, HIV+ children will demonstrate decreased structural connectivity (low FA, high MD) in WM tracts within the DMN, as well as the basal ganglia, somatosensory and salience networks. Based on our voxelwise DTI results, we will also observe decreased mean structural connectivity in HIV+ children within functional networks that involve the IFOF, ILF, superior corona radiata, ATR and FM tracts. These networks include: visual (lingual gyrus), ventral default mode network (vDMN), visual (occipital lobe), somatosensory, salience, auditory, motor, executive, basal ganglia, posterior default mode network (pDMN)
2) Based on our voxelwise DTI results at age 7, HEU children will have increased structural connectivity (high FA, low MD) compared to HUU children in RSNs where the posterior corona radiata and CST are present. The implicated RSNs include vDMN, somatosensory, pDMN, dorsal attention (dATT), salience, auditory, motor and basal ganglia.

2. BACKGROUND/LITERATURE REVIEW

2.1 HIV and ART

The brain environment is protected from pathogens as well as toxic compounds by the BBB. HIV invades the brain in a Trojan-horse-like manner as the virus infects peripheral monocytes and lymphocytes that transport the virus across the BBB (Boissé, Gill, & Power, 2008). Upon entering the brain, the virus infects macrophages, microglia and astrocytes. Many strains of HIV exist, and most neuroimaging studies of HIV have been performed in the USA and Europe where HIV-1 clade B is prevalent. HIV-1 clade C, which is most prevalent in Africa where approximately 90% of HIV+ children in the world reside, has received less attention (HIV.gov, 2018). These strains have been noted to have distinct strucutural differences (Gnanakaran et al., 2007) which suggests they may illicit different effects.

Though classified as a sexually transmitted infection, HIV can be transmitted from one person to another via several non-sexual ways, including direct blood contact (e.g. syringes and/or blood transfusions), and vertical transmission also referred to as mother to child transmission (MTCT) (CDC, 2017). MTCT can take place *in utero*, especially if the mother is immunocompromised, at delivery or during breastfeeding. MTCT is characterized in the child by a high viral load and poor prognosis with a life expectancy of 12-24 months in untreated infants (Attia et al., 2009). Several measures can be taken to prevent MTCT, including administration of ART during pregnancy which can lower maternal viral load and increase cluster of differentiation 4 (CD4+) count. Furthermore, opting for a caesarean section as opposed to natural birth reduces the chance of the baby coming into contact with the mother's blood and vaginal secretions while migrating through the birth canal. Breastfeeding is recommended in HIV+ mothers because of its substantial benefit to the infant. However, if the mother is not on treatment and/or not adhering to treatment guidelines, it poses a risk as HIV has been detected in breastmilk, and cracked and/or bleeding nipples can lead to transmission (Attia et al., 2009).

The onset of neuropathology due to HIV can occur at any stage after infection; however, most have been observed during the acquired immune deficiency syndrome (AIDS) stage because of increased immunosuppression. Several mechanisms caused by the virus (such as encephalopathy) may lead to brain damage or neurodevelopmental delay in children. HIV associated delays are characterised by

failure to reach certain milestones, such as motor, language or cognitive (Van Rie et al., 2007). Paediatric neurological disease is likely to develop if the child has a high viral load in CSF and/or high maternal viral load at the time of delivery.

Antiretroviral drugs (ARVs) work by interrupting multiple stages in the virus' replication cycle (Arts & Hazuda, 2012; Maartens et al., 2014) They can be classified into 5 major groups: (1) Fusion inhibitors prevent the binding of the virus onto the host cell; (2) reverse transcriptase inhibitors inhibit the formation of viral DNA; (3) integrase inhibitors prevent the integration of viral DNA into the host genome; (4) protease inhibitors inhibit the enzyme protease from forming infectious viral proteins and (5) multi-drug combination products that combine drugs from more than one class into a single product (Arts & Hazuda, 2012; Maartens et al., 2014) cART or Highly Active Antiretroviral Therapy (HAART) was introduced in 1996 (Berger, 1996). HAART combines at least two drugs from different antiretroviral classes to suppress the virus. This is done to prevent the virus from becoming resistant to one type of antiretroviral drug.

Though cART has significantly reduced MTCT and HIV encephalopathy, ARVs differ in their ability to penetrate the BBB. A central nervous system (CNS) penetration effectiveness (CPE) rank is a score that quantifies penetration of an ARV into the CNS (Letendre et al., 2009). Therapies with a low molecular weight and low protein binding rate have better penetration across the BBB (Ene et al., 2011). Reverse transcriptase inhibitors, particularly Zidovudine, tend to penetrate the BBB at higher concentrations (Ene et al., 2011). In theory therapies with a high CPE should lead to better CNS viral RNA suppression (Letendre et al., 2009). Low CPE therapies allow for continual replication of the virus in the CNS and, ultimately, the formation of drug resistant populations. These drug resistant populations cause continued neurocognitive impairment regardless of cART administration.

Though high CPE therapies have been associated with better neurocognitive outcomes (Carvalhal et al., 2016; Eisfeld et al., 2013) there have been studies that have shown an inverse association. This leads to the concern of ARVs and their potential neurotoxic effects (Shah et al., 2016). Early ART has shown significant neuroprotective effects, however the effects of long-term exposure to ARVs are still an area that is understudied. Negative neuropsychiatric effects, including depression and psychosis, have been associated with intake of several different ARVs (Shah et al., 2016). Some of the ARVs have been associated with peripheral nervous system

damage which reinforces concerns of CNS damage. Others, as part of their mode of action, alter the concentration of signalling molecules and enzymes in the CNS leading to neuronal damage (Streck et al., 2008).

2.2 MAGNETIC RESONANCE IMAGING

Since the mid-1980s, MRI has been an extremely powerful tool in both research and medical care. It has been especially useful *in vivo* for non-invasive neuroimaging of different aspects of the brain in both health and disease. MRI provides a range of information about the brain, from structure and function to metabolic function.

The underlying principle of MRI is to measure the net electromagnetic energy transmitted by atoms in the body (Dua & Singh, 2010; Kumar, 2014). For an atom to have a net magnetic energy or be regarded as 'MR active', it needs to contain an odd number of nucleic particles (sum of protons and neutrons), otherwise their spins (their magnetic momenta) would cancel each other out. Approximately 85% of the human brain is made up of water molecules which contain two hydrogen atoms and most importantly one proton within each of their nuclei, hence the frequent use of hydrogen in MRI.

The components of an MRI scanner include radiofrequency (RF) coils, gradient coils, and a large magnet generating a static magnetic field of high strength typically 1.5T, 3T or higher. The external/static magnetic field ($\mathbf{B_0}$) is applied in the z-plane which is typically in the inferior-superior orientation of the subject and is also referred to as the longitudinal direction. The xy-plane correspond to the transverse direction (Dua & Singh, 2010). When placed in an external magnetic field the magnetic momenta of the spins align themselves with the $\mathbf{B_0}$. The rate at which the spins precess in a direction of the main field' lines is known as Larmour frequency. Each nucleus has a unique frequency at which its particles precess about the external magnetic field and can be given by the Larmour equation below.

$$\omega_0 = \gamma B_0$$

γ is the precessional frequency of the magnetic spins of a specific nucleus (e.g. Hydrogen nucleus) at 1T and is known as the gyromagnetic ratio. To achieve magnetic

resonance, an RF pulse ($\mathbf{B_1}$) (also known as excitation pulse) with a frequency matching Larmour frequency is applied at an angle (flip-angle) with respect to $\mathbf{B_0}$ which causes the spins to now precess about $\mathbf{B_1}$ direction (e.g., in the transverse plane if the flip-angle is 90 degrees). The magnitude of the flip-angle is dependent on the amplitude and duration of the RF pulse. When the RF pulse is terminated, the spins will go back to precessing about $\mathbf{B_0}$. Two independent time constants are measured here, the time it takes for the magnitude of net magnetization to return to at least 63% of longitudinal magnetization (T_1 recovery time) as well as the time it takes for at least 63% of the transverse magnetization to be lost (T_2 decay time). Figure 1 shows T_1 recovery and T_2 decay behavior over time. These times are constant for different tissues and together with the different densities of protons within the tissues, are what create image contrast. The signal is read by a receiver coil which measures the transverse magnetization until it has completely decayed.

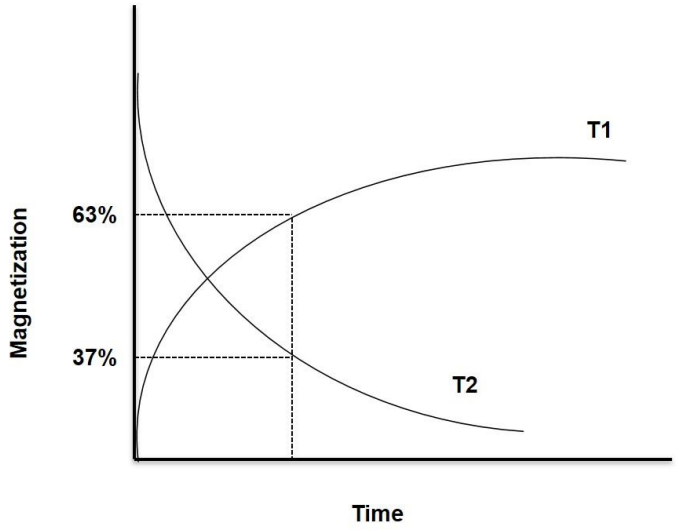

Figure 1: T1 recovery time and T2 decay time constants. The magnetization grows in the z-plane as it decays in the xy-plane. T2 is typically shorter than T1.

To select a specific slice and further localize the signal within the slice multiple gradient fields (**G**) are applied in different directions. For slice selection a G_{ss} is applied in a direction of the $\mathbf{B_0}$ field. The gradient field creates and off-set ($|\mathbf{B_0}| \pm G_{ss}$), with $|\mathbf{B_0}|$ measured in the middle of the scanner (isocenter). This means that there is a variability in the magnetic field strength experienced by the spins dependending on their location. Because we know that the amplitude of the effective magnetic field is changing in a predictable linear fashion,e.g., higher amplitude at the top of the head, 0 at the isocenter and lower at the neck, we can predict the frequency of the spins at any

location that we want to image and apply an RF pulse at that frequency to achieve resonance. Further, gradients can be applied in other directions to localize regions within the selected slice. A frequency encoding gradient is applied in a direction perpendicular to the slice selection gradient and a phase encoding gradient is applied in a direction that is perpendicular to both (Dua & Singh, 2010).

2.3 DIFFUSION TENSOR IMAGING

DTI measures describe the structural organisation of WM of the brain typically, though they can be used to describe GM structural organisation as well (Pfefferbaum et al., 2010; Rulseh et al., 2013). This imaging modality has many applications and has been used to study WM growth from as early as 8 weeks gestational age (Feldman et al., 2010), through childhood to adulthood (Lebel et al., 2008). It has been used to demonstrate brain injury in many disorders such as acute stroke (Chen et al., 2008), multiple sclerosis (Sbardella et al., 2013) and hepatic ischemia. DTI also has the potential to be used as a prognostic tool; it has been used to demonstrate how DTI parameters in poor readers changed after therapy, ultimately improving their reading skills (Feldman et al., 2010).

In WM, diffusion is anisotropic i.e. dependent on tissue orientation. The 3x3 diffusion tensor (D) fully describes the mobility of molecules in each direction and the relationship between these directions (Mori & Zhang, 2006). To find components of this tensor, gradient-field pulses (so called diffusion gradients) are introduced after the excitation component of the MRI sequence. Their role is to re-phase stationary molecules, while causing a net phase shift proportional to the molecule's displacement along the gradient direction for molecules that are moving due to diffusion. This phase shift causes signal attenuation dependent on the degree of diffusion in the direction of the gradient (Mori & Zhang, 2006). By repeating this measurement for many different gradient directions, the different components of the diffusion tensor can be calculated for each voxel. Although, in a simplest diffusion model (where a symmetric tensor D, i.e., $D_{ij}=D_{ji}$) a minimum of 6 gradient directions are required to fully solve for all components of D, most DTI sequences typically use between 16 and 64 gradient directions. This is because more gradient directions which ultimately means more diffusion weighted images result in a more accurate calculation of D (Ni et al., 2006).

Within each voxel, diffusion can be characterized by four scalar parameters, calculated from the eigenvalues (L1, L2, L3) of the diffusion tensor, namely, fractional anisotropy (FA), mean diffusivity (MD), axial diffusivity (AD) and radial diffusivity (RD) (O'Donnell & Westin, 2011b). Each eigenvalue corresponds to one of the eigenvectors (V1, V2, V3). Geometrically, the diffusion tensor forms an ellipsoid with three main axes oriented in directions (defined by the eigenvectors) that translate to the extent (defined by eigenvalues) of diffusivity in that direction (O'Donnell & Westin, 2011b) (Figure. 2).

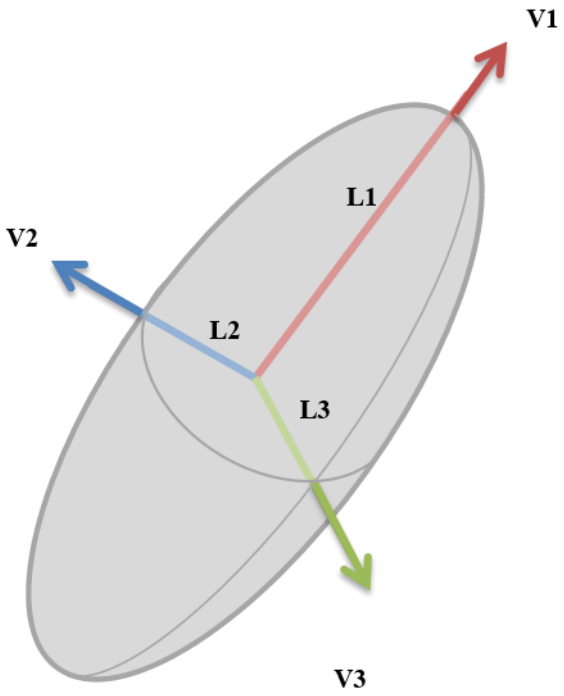

Figure 2: Diffusion tensor ellipsoid with three eigenvectors (V1, V2 and V3) and three eigenvalues (L1, L2 and L3), corresponding to the ellipsoid's main axes and radii.

The longest axis of the ellipsoid is the direction with the maximum diffusion and describes AD. Some studies have noted AD to increase with brain maturation and decrease in axonal damage (O'Donnell & Westin, 2011b) while other studies have noted very little to no change in AD with age (Lebel et al., 2008). WM has high AD values and low values reflect axonal damage along the WM tract. Conversely, RD describes the amount of diffusion perpendicular to the WM axons. Myelin, which surrounds an axon, hinders perpendicular diffusion. Thus high RD values indicate WM damage due to de- or dysmyelination (Feldman et al., 2010). Demyelination refers to a loss of myelin whereas dysmyelination refers to abnormal formation or malfunctioning of myelin. RD may also be influenced by changes in axonal diameter

or density (Tromp, 2016). FA is a normalized standard deviation of the eigenvalues and represents the extent to which diffusion is anisotropic (Dietrich et al.,, 2010; Hagmann et al., 2006; O'Donnell & Westin, 2011b). It is a value between 0 and 1, where 0 means the diffusion is isotropic and 1 means the diffusion is only along one axis and is fully restricted along perpendicular directions. FA is influenced by axonal packing where dense packing would mean a lower intercellular space and higher restriction on diffusion of water thus increasing FA (Hoeft et al., 2007). Increased myelination results in denser axonal packing (Alexander et al., 2011). FA is generally used as an indicator of WM integrity. MD, which is independent of anisotropy, demonstrates the average movement of water within the WM voxel and can be interpreted as a general indicator of WM maturation and/or injury (Basser & Pierpaoli, 1996). Studies have shown that MD decrease with age (Lebel et al., 2008). Table 1 shows how biological changes influence the different DTI scalar parameters individually. Though FA and MD are both individually sensitive to microstructural changes, it is advisable to include other DTI scalars in any analysis to best interpret the results.

Table 1: How biological changes influence each DTI scalar parameter (*adapted from* (Tromp, 2016))

	AD	RD	FA	MD
WM maturation	↑	↓	↑	↓
Increased myelination	-	↓	↑	↓
Dense axonal packing	-	↓	↑	↓
Axonal damage	↓	↑	↓	↑
De- or dysmyelination	-	↑	↓	↑

DTI also allows for 3-dimensional fibre tracking/tractography demonstrating WM structural connectivity. Fibre tracking is achieved by following a WM fibre bundle from voxel to voxel using each voxel's axial diffusion direction until any one of the stopping criteria is reached. One of three tracking methods is employed in tractography: 1) deterministic 2) probabilistic and 3) mini-probabilistic. We used both probabilistic and mini-probabilistic methods (see methodology for detailed description) in the current study.

WM tracts implicated in studies of paediatric cohorts include the CST and corona radiata, IFOF, ILF, cingulum, superior longitudinal fasciculus (SLF), ATR and FM (Ackermann et al., 2016; Fuentes et al., 2016; Hoare et al., 2015; Jankiewicz et al., 2017). A cross-sectional study on HIV+ ART-naïve South African adolescents (n = 12 HIV+, age range = 8-12 years) examined neuropsychological performance and WM integrity compared to uninfected controls (Hoare et al., 2012). The HIV-infected children performed poorly in motor and executive functioning as well as processing speed, compared to uninfected controls. Furthermore, the HIV-infected children had lower FA and higher RD in the corpus callosum, and higher MD and RD in the SLF, compared to uninfected controls. Though ART treated children without HIV encephalopathy show better WM integrity than ART naïve children with HIV encephalopathy, ART treated children continue to exhibit axonal damage (Hoare et al., 2015). Another study in ART-treated youth showed higher viral load being associated lower cognitive performance, lower FA in the IFOF and uncinate fasciculus and higher MD in the FM compared to uninfected controls (Uban et al., 2016). Li et al also found lower FA in corpus callosum, superior and posterior corona radiata and SLF in ART-treated adolescents compared to uninfected controls (Li et al., 2015). Even in children initiating ART before 2 years of age, regional FA reductions and MD increases are still evident, although the corpus callosum appears to be spared (Jankiewicz et al., 2017). FA reductions and MD increases are largely attributable to greater RD, suggesting an effect of HIV/ART on myelination (Hoare et al., 2012). Another cross-sectional study on cART-treated South African adolescents (n = 50 HIV+, age range = 6-15 years) showed that, increased viral load is associated with higher MD, RD and lower AD values in the corpus callosum as well as the SLF. Furthermore, lower FA in the fornix, CST, cerebellar peduncle, cingulum and superior front-occipital fasciculus (SFOF), was associated with reduced albumin and haemoglobin (Hoare et al., 2015).

These studies not only show continued HIV-associated damage albeit treatment, some also attempt to make links between neuropsychological, neurocognitive, clinical and WM alterations in HIV+ adolescents and youth. The current study would be useful in demonstrating whether is a relationship between functional and structural damage. Table 2 has a summary of DTI studies performed on HIV+ children.

Table 2: Summary of studies performed on HIV+ youth using DTI

Study ID	Aim	N; age range; ART	Selected results
(Hoare et al., 2012)	Examine neuropsychological performance and WM integrity in ART-naïve children	12 HIV+, 12 controls; 8-12 years; ART-naïve	Compared to uninfected controls, HIV+ children had lower FA and higher RD in the corpus callosum. They also had higher MD in and RD in the SLF Lower FA in the CC was associated with poorer test scores.
(Hoare et al., 2015)[a]	Examine correlation between clinical and WM damage in ART-treated children	50 HIV+; 6-15 years; ART-treated	Lower haemoglobin was associated with lower FA in the fornix, CST, cingulum, superior fronto-occipital fasciculus, cerebellar peduncle and uncinate fasciculus. Higher viral load was associated with increased MD in the corpus callosum and splenium and I the SLF

(Hoare et al., 2015)[b]	Examine HIV and ART effects on WM integrity and neurocognitive function.	75 HIV+, 30 controls; 6-16 years; 41 ART-treated	Compared to uninfected controls: • HIV+ children had lower FA and AD in the cerebral peduncles and fornix and higher MD and RD in the superior corona radiata • HIV+ ART-treated children had lower FA in the corpus callosum and fornix ART-naïve children showed higher MD in the external capsule and fornix, compared to ART-treated children
(Li et al., 2015)	Investigate WM microstructural integrity in adolescents with vertically transmitted HIV.	15 HIV+, 26 Controls; 13 – 17 years; ART-treated	Compared to controls, HIV+ children demonstrated reduced FA in the corpus callosum, superior & posterior corona radiata, SLF, frontal & parietal WM, and pre-/postcentral gyrus.

(Uban et al., 2016)	Investigate association between HIV disease severity and structural connectivity and cognition.	40 HIV+, 314 controls; 11-21 years; ART-treated	Among HIV+ children: higher viral load was associated with poorer cognitive performance High VL was associated with lower FA in the IFOF and uncinate High CD4% was associated with lower AD in the FM High VL was associated with higher MD in the FM
(Ackermann et al., 2016)	Examine effects of early ART on WM integrity	39HIV+; 5years; ART-treated (26 before 12 weeks)	Compared to uninfected controls, HIV+ children had lower FA in the internal capsule and higher MD in the SLF, CST, IFOF, FM and uncinate fasciculus
(Jankiewicz et al., 2017)	Examine the effects of HIV and exposure in uninfected children	65HIV+, 46 controls (19 HEU); 7 years; ART-treated	Compared to uninfected controls, HIV+ children had lower FA in the IFOF and ILF, and higher MD in the superior corona radiata, ATR, FM, IFOF and ILF. HEU children had higher FA in the posterior corona radiata

2.4 RESTING STATE FUNCTIONAL MRI IN HIV

RS-fMRI is used to assess functional connectivity (FC), which is characterized by temporal correlations in neuronal activity patterns of anatomically separate GM regions. The main RS networks of the brain include the visual, motor, sensorimotor, attention, salience, executive control and default mode network (DMN). There are typical, though not strict, boundaries for each network and others have been seen to split or divide within these boundaries.

Most RS-fMRI studies in HIV have focused on adults (Ann et al., 2016; Chaganti et al., 2017; Ortega et al., 2015; Wang et al., 2011). Despite viral suppression (both plasma and CSF), lower intranetwork connectivity has been reported in the salience and executive control networks (Chaganti et al., 2017) and between the bilateral precuneus and prefrontal cortex, in adults with HIV-associated neurocognitive disorder (HAND) (Ann et al., 2016). In the lateral occipital cortex, which plays a role in visual attention, lower RS FC is already evident within a year of infection (Wang et al., 2011). In contrast, Janssen et al. (2016) found no differences in RS connectivity in subcortical regions between HIV+ patients on long-term cART and uninfected controls. Their results were in agreement with those of Ortega et al. (2015) who found similar findings within DMN connectivity in patients on cART compared to healthy controls, and higher functional connectivity within the ventral attention network in patients on cART compared to cART naïve patients (Ortega et al., 2015). Combined, these studies suggest that ART may be neuroprotective for functional networks.

RS-fMRI studies in children with perinatally acquired HIV are limited. To date, the only paper examining RS-fMRI in paediatric HIV found patterns of connectivity reflecting developmental delay in youth with greater disease severity, including poorer functional connectivity within the DMN (Herting et al., 2015). Within our cohort, we found evidence at age 7 years of developmental delay, characterised by greater short-distance and weaker long-distance connectivity, in HIV+ children compared to uninfected controls (Toich et al., 2018). Although no functional connectivity differences were observed at this age within any of the 12 resting state networks (RSNs) identified via Independent Component Analysis (ICA), seed based analysis demonstrated lower functional connectivity within the DMN (Toich et al., 2018). Other networks showed HIV/ART related effects, specifically lower between network

connectivity in the somatosensory, executive control and salience networks. Both Herting *et al* (2015) and Toich *et al* (2018) also observed increased functional connectivity associated with higher disease severity. A similar pattern was observed in HIV+ adults compared to uninfected controls (Thomas et al., 2013)

3. METHODOLOGY

3.1 STUDY COHORT

A total of 125 7-year-old children participated in the current study. Data from eighteen were excluded due to motion artefacts in more than half of the DWI volumes. Thus, we present data from a total of 107 (89 Xhosa/18 Cape Coloured) 7-year-old children. The HIV+ children have been followed since birth at the Family Clinical Research Unit (FAMCRU), Tygerberg Children's Hospital, in Cape Town, South Africa. HIV+ children were recruited from the CHER trial (Cotton et al., 2014) which followed the children till the age of 5 years. For the CHER trial, the children were randomly distributed into different treatment arms. Some began treatment between 6 and 12 weeks of age, while others began after 12 weeks of age. (Cotton et al., 2014).

The HIV-uninfected children were recruited from a parallel vaccine study (Madhi et al., 2010). The uninfected group is further subdivided into those born to HIV+ mothers (exposed uninfected, HEU) and those born to uninfected mothers (unexposed uninfected, HUU). As part of the current study, the children are being followed with neurocognitive testing and neuroimaging at ages 5, 7, 9 and 11 years. All HIV+ children are on ARV therapy. The ART regimens for all treatment arms consist of ZDV + Lamivudine (3TC, Epivir) + Lopinavir + Ritonavir (LPV/r, Kaletra). The sample demographics are summarised in Table 1.

Table 3: Summary of study population

		HIV+	HUU	HEU
Demographics				
N		61	27	19
Ethnicity	Xhosa, N (%)	52 (85)	19 (70)	18 (95)
Gender	Female, N (%)	33 (54)	13 (48)	8 (42)
Age at scan	Mean±SD	7.21 ± 0.13yrs	7.3 ± 0.20yrs	7.20 ± 0.11yrs
Clinical measures at baseline				
CD4 count (cells/mm^3)		1,764 ± 869		
CD4 %		33 ± 11		
CD4/CD8		1.28 ± 0.73*		
CD8 count (cells/mm^3)		1,666 ± 1,097*		
CD8 %		31 ± 10		
High VL (>750,000) (N)		36		
Low VL (400-750,000) (N)		25		
Suppressed VL (<400) (N)		0		
Clinical measures at scan				
CD4 count (cells/mm^3)		1,128 ± 464		
CD4 %		37 ± 6		
High VL (>750,000) (N)		0		
Low VL (400-750,000) (N)		3		
Suppressed VL (<400) (N)		58		
Treatment-related measures				
ART initiation before 12 weeks (N)		48		
Age at ART interruption (weeks)		71 ± 27†		
Duration of ART interruption (weeks)		65 ± 89		

* 1 subject missing; † 12 subjects were not interrupted and received ART continuously.

3.2 MRI ACQUISITION

Neuroimaging data were acquired at age 7 years according to protocols that were approved by the Human Research Ethics Committees of both the Universities of Cape Town and Stellenbosch. Participants were scanned at the Cape Universities Brain Imaging Centre (CUBIC) adjacent to Tygerberg Hospital, using a 3T Siemens Allegra scanner (Siemens, Erlangen, Germany) with a single channel head coil. Structural T1-weighted (T1w) images were acquired using a volumetric navigated multi-echo magnetization prepared rapid gradient echo (MEMPRAGE) sequence (voxel size = 1.3×1.0×1.0 mm^3 , FOV = 224×224×144 mm^3 , TR = 2530 ms, TI = 1160 ms, TEs = 1.53/3.19/4.86/6.53 ms, flip angle = 7^o), followed by 2 DTI acquisitions with opposite phase encoding (Anterior-Posterior, Posterior-Anterior; AP, PA) directions using a prospectively motion-corrected navigated twice-refocused spin echo sequence with 5 reacquisitions (Alhamud et al., 2012). Acquisition parameters for diffusion were: TR/TE 10100/86ms, 72 slices, 2×2×2mm^3, FOV = 224×224×144 mm^3, 30 non-collinear diffusion directions, b=1000s/mm^2, and four non-diffusion-weighted (b0) acquisitions.

3.3 IMAGE PROCESSING

All data was pre-processed using the software package Tolerably Obsessive Registration and Tensor Optimization Indolent Software Ensemble (TORTOISE) version 3.1 (Pierpaoli et al., 2009) and tractography was performed using the Functional And Tractographic Connectivity Analysis Toolbox (FATCAT) (Taylor & Saad, 2013) within the Analysis of Functional Neuroimages (AFNI) toolbox (Cox, 1996).

3.3.1 PRE-PROCESSING

Before tractography and statistical analyses, all participants' datasets were pre-processed using a series of in-house scripts. For each participant DICOMs were

converted to a NIFtI readable format for TORTOISE and T2w anatomical images were created from the T1w images that were acquired during scanning. The T2w image is created using AFNI's *fat_proc_imit2w_from_t1w* function. Subsequently, manual visual quality control of all diffusion weighted images (DWIs) was performed and distorted volumes discarded. TORTOISE's *DIFFPREP* function was used to correct DWI artefacts such as motion and eddy distortion by using each participant's T2w anatomical image and a registration settings file. We used the T2w anatomical image because it has the structure and intensity of the population being studied thus helped in removing distortions. The registration settings file contained settings on which corrections would be made to the data.

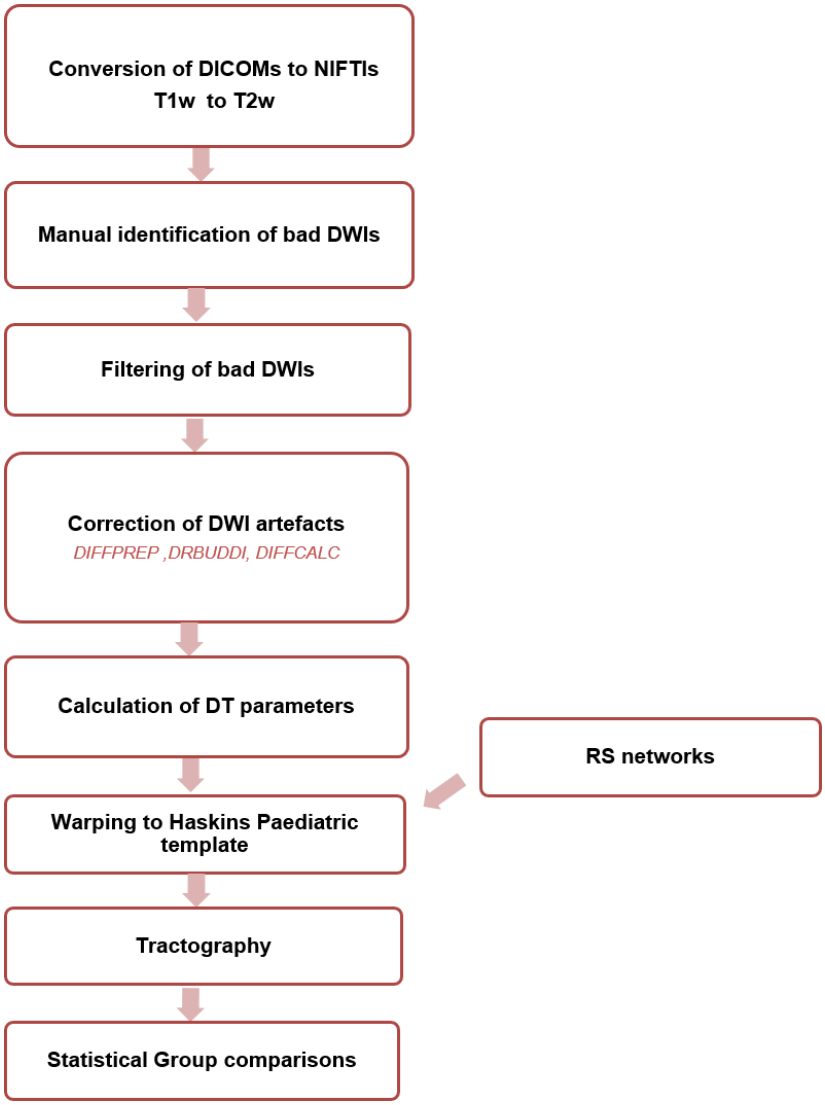

Figure 3: Data processing pipeline.

TORTOISE's *DRBUDDI* function was used to correct DWI distortion and to combine the 2 opposite phase encoding directions (AP,PA). This function used the AP and PA data as well as the T2w anatomical image as input. Because *DRBUDDI* uses *DIFFCALC*'s output to internally apply motion and eddy current distortion correction together with deformation fields accounting for EPI distortions to yield the final corrected data, it can only be performed after *DIFFPREP*.

Following *DRBUDDI*, the results were converted into usable NIFTIs using TORTOISE's *DIFF_CALC* and exported to AFNI. To estimate diffusion tensors and

DTI parameters AFNI's *fat_proc_dwi_to_dt* function was used. The T2w anatomical image was used as the reference image to accomplish alignment as well as the correct orientation of the DWI datasets. The output consisted of the estimated parameters and included: all three eigenvalues (L1, L2, L3), all three eigenvectors (V1, V2, V3), FA, MD, AD and RD. Another part of the output created using by the *3dDWUncert* function part of *fat_proc_dwi_to_dt* is a file containing information on the uncertainty of the DTI parameters. Because the three eigenvectors are not perfectly orthogonal to one another there is room for errors, thus *3dDWUncert* calculates the bias and standard deviation of V1 with reference to V2 and V3 as well as the bias and standard deviation of FA.

Finally the DTI data and RSNs (described below) were warped using AFNI's *3dNwarpApply* which performed a non-linear 3D warp (AFNI, 2014) onto the Haskins paediatric brain atlas (Molfese et al., 2011) in order to select regions of interest (ROIs) and begin tractography. Because of the age driven morphology variability in both GM and WM the choice of brain atlas is very important. The Haskins paediatric brain atlas was created using data from participants between the age of 7 and 12 which made it a suitable choice for the current study. For the current study, we did not process any fMRI data to acquire the RSNs as these were already extracted using group ICA in a previous study (Toich et al., 2018). Toich *et al.* used both ICA and seed based analyses to examine functional connectivity in HIV+ children compared to uninfected controls. ICA analyses produce RSNs then explores functional connectivity within those boundaries whereas SCA analyses explore whole brain connectivity to one specific region (seed). A detailed description of pre-processing of RS fMRI is described (Toich et al., 2018).

Each RSN is made up of a set of GM regions (ROIs) (Table 4) and some of these regions belong to multiple RSNs. However, we masked the GM regions by applying the mask of the RS functional network they belong to. Thus, even if the GM region belongs to two or more networks, only a part of it is considered to be connected to another GM region within a particular network. With the DTI data warped to the RSNs, we identified the ROIs within each network using AFNI's *3dROIMaker*. The RSNs within which the tractography was performed are illustrated in Figure 4.

Table 4: The 12 RSNs and the GM regions that they comprise of.

Visual (lingual gyrus)

- Precuneus
- Cuneus
- Superior parietal cortex
- Lateral occipital cortex
- Pericalcarine
- Isthmuscingulate

vDMN

- Precuneus
- Cuneus
- Isthmuscingulate
- Inferior parietal cortex
- Fusiform
- Inferior temporal cortex
- Parahippocampal cortex
- Hippocampus
- Amygdala
- Middle temporal cortex
- Medial orbitofrontal cortex
- Superior parietal cortex
- Entorhinal

Visual (occipital lobe)

- Cuneus
- Fusiform
- Pericalcarine
- Lateral occipital cortex
- Inferior parietal cortex
- Superior parietal cortex
- Inferior temporal cortex

Somatosensory network

- Precuneus
- Precentral gyrus/cortex
- Postcentral gyrus/cortex
- Paracentral gyrus/cortex
- Posterior cingulate cortex
- Insula
- Thalamus
- Putamen
- Superior temporal cortex
- Superior frontal cortex
- Supramarginal cortex
- Superior parietal cortex

Posterior DMN

- Precuneus
- Cuneus
- Paracentral gyrus/cortex
- Posterior cingulate cortex
- Inferior parietal cortex
- Superior parietal cortex
- Isthmuscingulate
- Posterior cingulate cortex

Dorsal attention network

- Precuneus
- Superior parietal cortex
- Inferior parietal cortex
- Superior frontal cortex
- Inferior temporal cortex
- Supramarginal cortex
- Fusiform
- Caudal middle frontal cortex

- Rostral middle frontal cortex
- Medial orbitofrontal cortex
- Precentral gyrus/cortex
- Postcentral gyrus/cortex
- Paracentral gyrus
- Posterior cingulate cortex
- Parsopercularis

Salience network

- Precuneus
- Caudate
- Insula
- Putamen
- Pallidum
- Medial orbitofrontal cortex
- Superior temporal cortex
- Superior frontal cortex
- Supramarginal cortex
- Precentral gyrus/cortex
- Postcentral gyrus/cortex
- Parsopercularis
- Parstriangularis
- Caudal anterior cingulate cortex
- Rostral anterior cingulate cortex
- Rostral middle frontal cortex
- Posterior cingulate cortex
- Transverse temporal cortex
- Lateral orbitofrontal cortex

DMN

- Precuneus
- Hippocampus
- Medial orbitofrontal cortex
- Lateral orbitofrontal cortex
- Superior frontal cortex
- Inferior parietal cortex
- Caudal middle frontal cortex
- Rostral middle frontal cortex
- Rostral anterior cingulate cortex
- Isthmuscingulate

Auditory network

- Precuneus
- Fusiform
- Isthmuscingulate
- Inferior parietal cortex
- Superior frontal cortex
- Lateral occipital cortex
- Superior temporal cortex
- Inferior temporal cortex
- Parsopercularis
- Parsobitalis
- Parstringularis
- Lateral orbitofrontal cortex

Motor network

- Precuneus
- Cuneus
- Putamen
- Insula
- Thalamus
- Superior temporal cortex
- Postcentral gyrus/cortex
- Precentral gyrus/cortex
- Supramarginal cortex
- Parsopercularis
- Isthmuscingulate
- Superior frontal cortex

- Supramarginal cortex
- Caudal middle frontal cortex
- Lateral occipital cortex

Executive network

- Precuneus
- Supramarginal cortex
- Inferior temporal cortex
- Middle temporal cortex
- Inferior parietal cortex
- Lateral orbitofrontal cortex
- Rostral middle frontal cortex
- Caudal middle frontal cortex
- Superior parietal cortex
- Superior frontal cortex
- Posterior cingulate cortex
- Isthmuscingulate
- Parsorbitalis
- Parstriangularis
- Parsopercularis
- Postcentral gyrus/cortex

Basal ganglia

- Caudate
- Ventral diencephalon
- Thalamus
- Pallidum
- Putamen

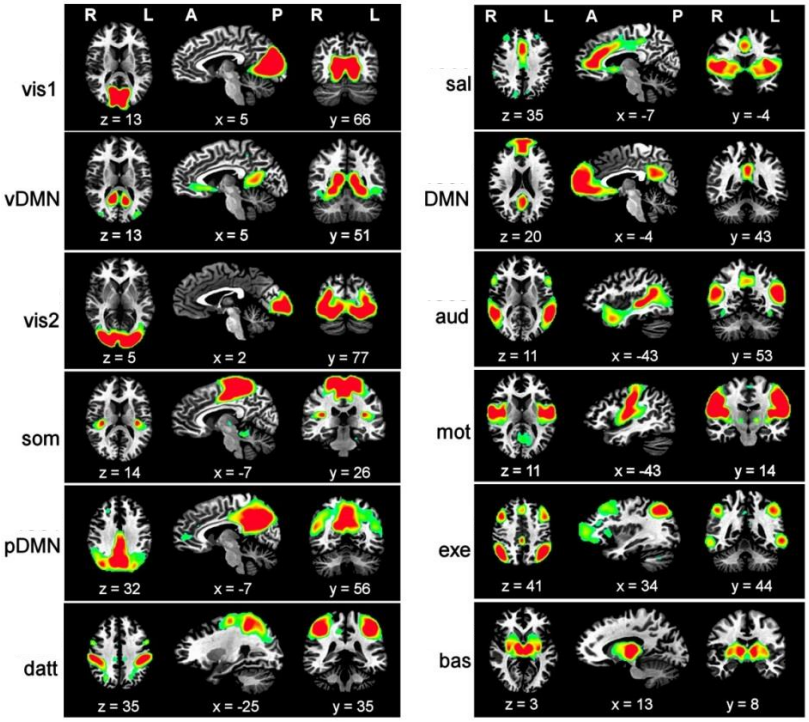

Figure 4: RSNs extracted from group independent component analysis (ICA): visual lingual gyrus (vis1); ventral default mode network (vDMN); visual occipital lobe (vis2); somatosensory (som); posterior default mode network (pDMN); dorsal attention (datt); salience (sal); default mode network (DMN); auditory (aud); motor (mot); executive (exe); basal ganglia (bas). Networks are overlaid on standard Talairach-Tournoux (TT) space (left = left) (adapted from (Toich et al., 2018)).

3.3.2 TRACTOGRAPHY

DTI tractography is performed by firstly selecting a specific number of seed points in a voxel (Descoteaux et al., 2007). Tracts will then propagate from voxel to voxel based on the AD direction in each voxel. Propagation continues until any one of the stopping criteria is reached which essentially means the tract likely does not pass through that voxel. Specifically stopping criteria in our study consisted of: angle threshold (turning angle>60º), FA threshold (FA< 0.2) and tract length (<20mm). The turning angle must be less than 60º to avoid making a U-turn during propagation of a tract. FA values in WM in children are at least 0.2 (Ghosh et al., 2017) thus a threshold of 0.20 ensures that tractography won't include regions that are not WM such as GM or CSF (Feldman et al., 2010). Lastly, the propagated WM bundle must be at least 20mm to be considered a tract.

AFNI's *3dTrackID* function was used to estimate the locations of WM associated with target ROIs and can run in one of three different modes; Deterministic (DT), Mini probabilistic (MINIP) and Probabilistic (PROB). DT tractography follows a tract from a seed point within a voxel to another voxel based on the principal direction of diffusion. This is only done once for a given dataset (Alexander et al., 2011). However, complications arise in a case where tracts cross within a voxel and the AD direction no longer represents the initial tract that was being followed (Feldman et al., 2010). PROB tractography (used in this study) avoids this problem by considering all possible directions a tract could take (Descoteaux et al., 2007). It is performed by selecting a seed point in a voxel, then selecting a random angle and direction for the tract to propagate considering the uncertainty of that direction. The uncertainty is considered using the uncertainty information file created by the *3dDWUncert* function previously. The tract propagates through each voxel until stopping criteria are met. Subsequently, a different but random angle and direction is chosen starting from the same initial seed point. Thus, a single seed point could have a thousand iterations of tracts propagating from it. MINIP tractography (Taylor et al., 2015) is a cross between DT and PROB tractography as it contains multiple seed points per voxel with less iterations. For our analysis, MINIP tractography was used for presentation purposes and outputs from PROB tractography for our statistical analyses. We used MINIP tractography for presenation because the output from PROB tractography does not allow for visualisation. Figures 5 and 6 show an example of a whole brain and intra-network tractography results respectively in a randomly selected control subject.

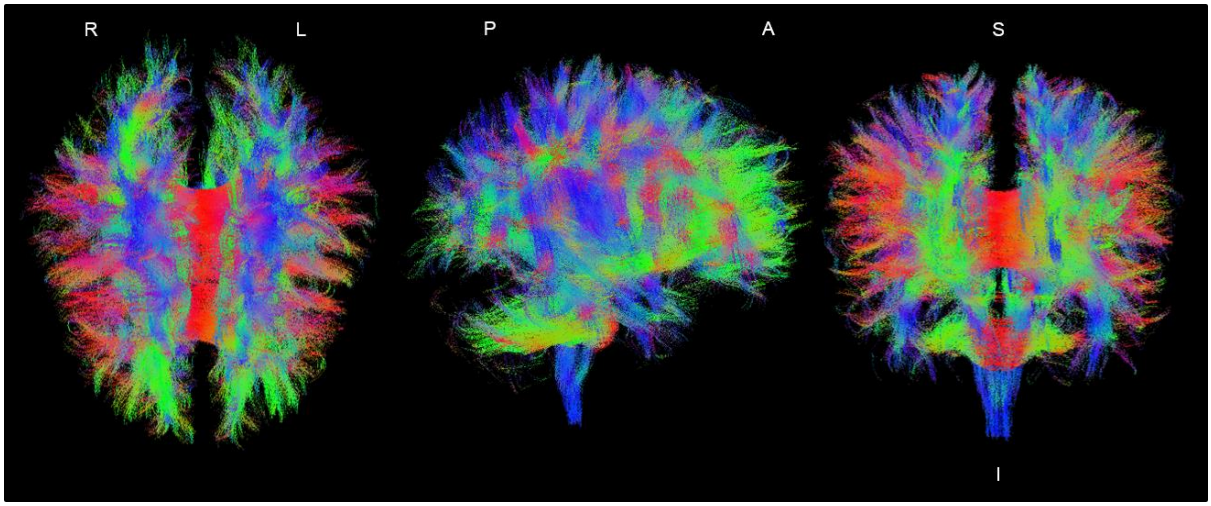

Figure 5: Whole brain WM tractography. The different colours denote the direction of the WM tracts: red = LR-direction; green = AP-direction; blue = SI-direction.

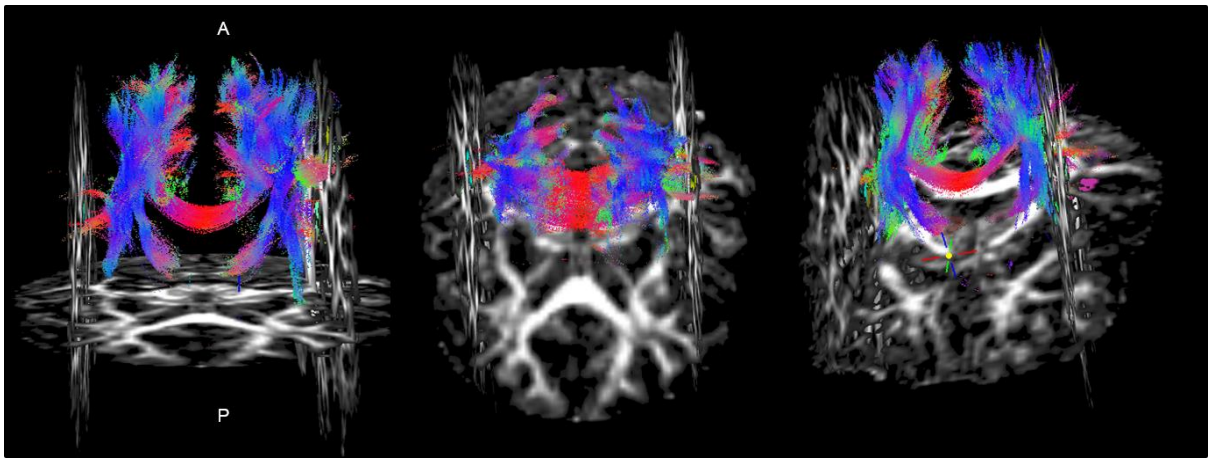

Figure 6: Example of WM tractography within the somatosensory network. The different colours denote the direction of the WM tracts: red = LR-direction; green = AP-direction; blue = SI-direction.

3.4 STATISTICAL ANALYSES

We extracted FA, AD, MD and RD, in FATCAT (version 1.1) for each tract connecting distinct ROIs within each RSN for each subject. Each functional network has a unique number of connections which is determined by the number of GM to GM connections within that network. We then exported this data to R statistical software (version 3.4.2) where we performed our statistical analyses. We ran two ANCOVA models. The first was the main investigation of the study: HIV+ children vs controls. The second model compares HEU to HUU children. In both of our models we controlled for gender and ethnicity. We used an alpha (α) significance level of p=0.01.

Furthermore, we corrected for multiple comparisons using the false discovery rate (FDR) method (Benjamini & Hochberg, 1995). This method allows for calculation of

the proportion of results meeting the significance criteria that are false positives when comparing independent samples. The method uses the number of tests (number of connections between two GM regions in our case), *m*, divided by the ranking (assuming p-values are arranged in descending order) of the calculated p-value, *i,* and multiplied by the p-value of the test, α, to calculate the adjusted p-value. We used an adjusted significance level of p=0.05.

3.5 Data visualization

We identified the tracts which the WM connections between GM regions belonged to in FSLView (version 5.0.9), using the JHU ICBM-DTI-81 White Matter Labels as well as the JHU White Matter Tractography Atlas (Hua et al., 2008; Mori et al., 2005; Wakana et al., 2007). Where the WM connection could not be identified they were recorded as 'WM connection'. Figures were generated, from a randomly selected control subject, using FreeView (version 5.3.0). Within each network with significant group differences, we extracted the GM region(s) between which WM connections showed significant differences between groups. Subsequently, we used our output from MINIP tractography to show the affected WM connections, which we overlaid on the GM regions. Furthermore, we included the WM tract to which the affected WM connections belonged to.

Our statistics tables report connections that showed statistically significant ($p<0.01$) group differences in FA and MD. We included the AD and RD values for those connections as well to distinguish which of the two, if not both, are driving the differences.

4. RESULTS

Comparisons of HIV+ children and controls revealed reduced FA and AD, as well as increased RD, within WM tracts in the somatosensory, salience, auditory and motor networks. The HIV+ children also showed higher MD and RD compared to controls within multiple tracts in the somatosensory, salience, DMN, basal ganglia and motor network.

Further, the HEU children demonstrated higher FA compared to HUU children within tracts in the posterior DMN, visual (occipital lobe and lingual gyrus), salience and motor networks.

We present plots and images of tracts of all results.

4.1 FA - HIV+ vs Control children

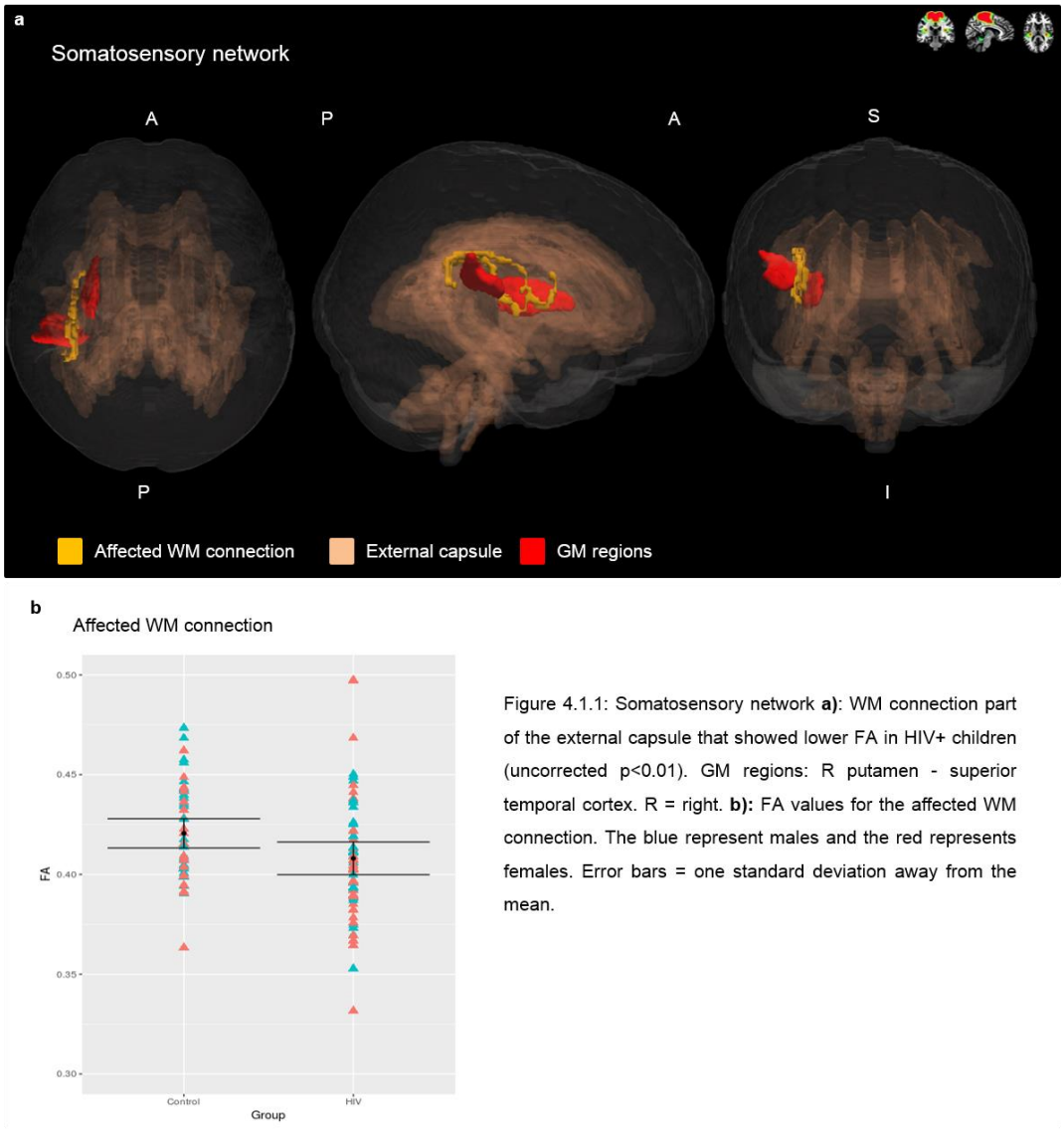

Figure 4.1.1: Somatosensory network **a)**: WM connection part of the external capsule that showed lower FA in HIV+ children (uncorrected p<0.01). GM regions: R putamen - superior temporal cortex. R = right. **b):** FA values for the affected WM connection. The blue represent males and the red represents females. Error bars = one standard deviation away from the mean.

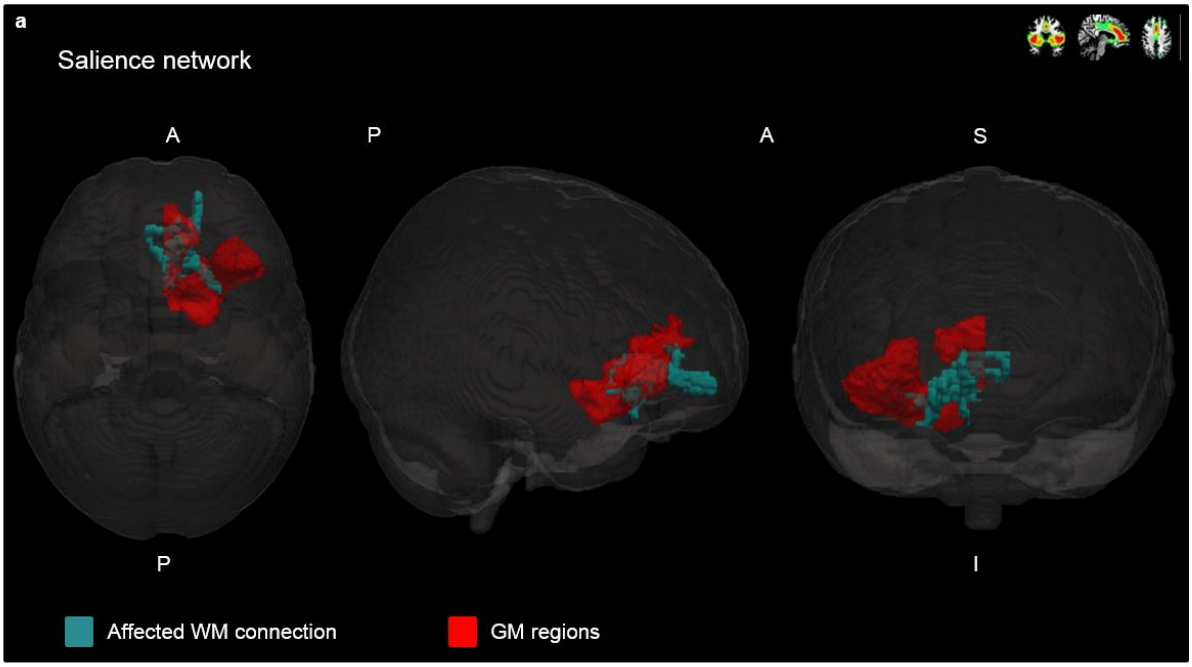

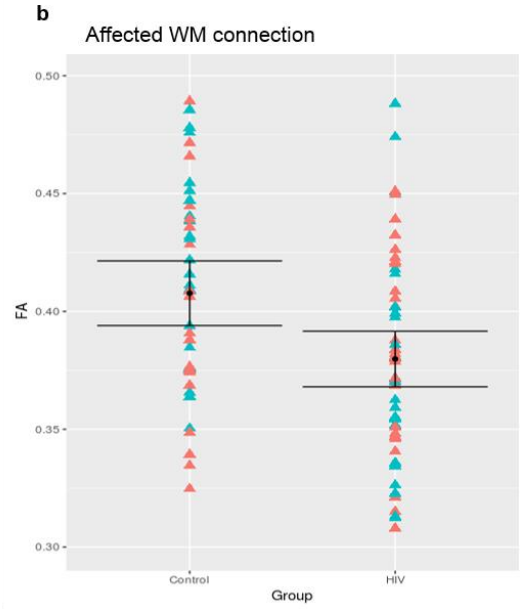

Figure 4.1.2: Salience network **a)**: Affected WM connection that showed lower FA in HIV+ children (uncorrected p<0.01) . GM regions: R lateral orbitofrontal cortex – rostral anterior cingulate cortex. R = right. **b):** FA values for the affected WM connection. The blue represent males and the red represents females. Error bars = one standard deviation away from the mean.

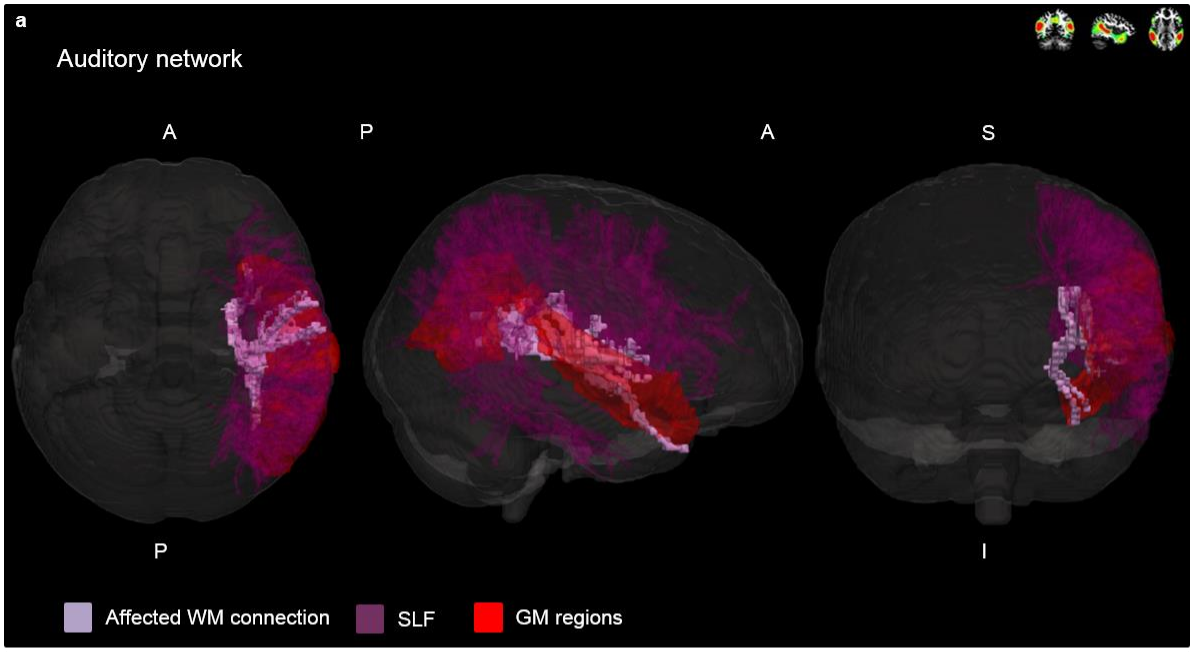

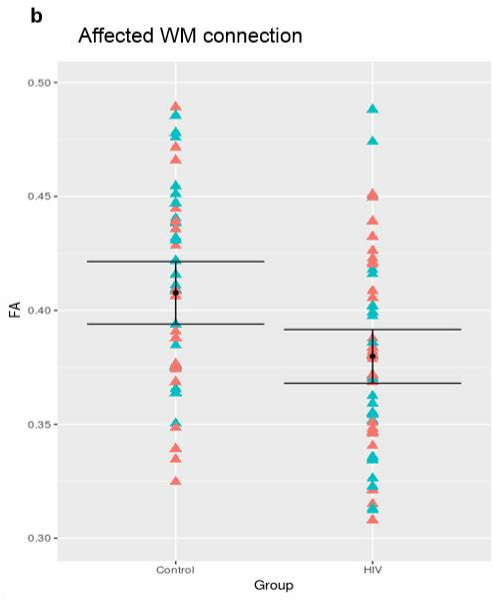

Figure 4.1.3: Auditory network **a)**: Affected WM connection part of the SLF that showed lower FA in HIV+ children (uncorrected p<0.01) . GM regions: R inferior parietal cortex – superior temporal cortex. R = right. **b):** FA values for the affected WM connection. The blue represent males and the red represents females. Error bars = one standard deviation away from the mean.

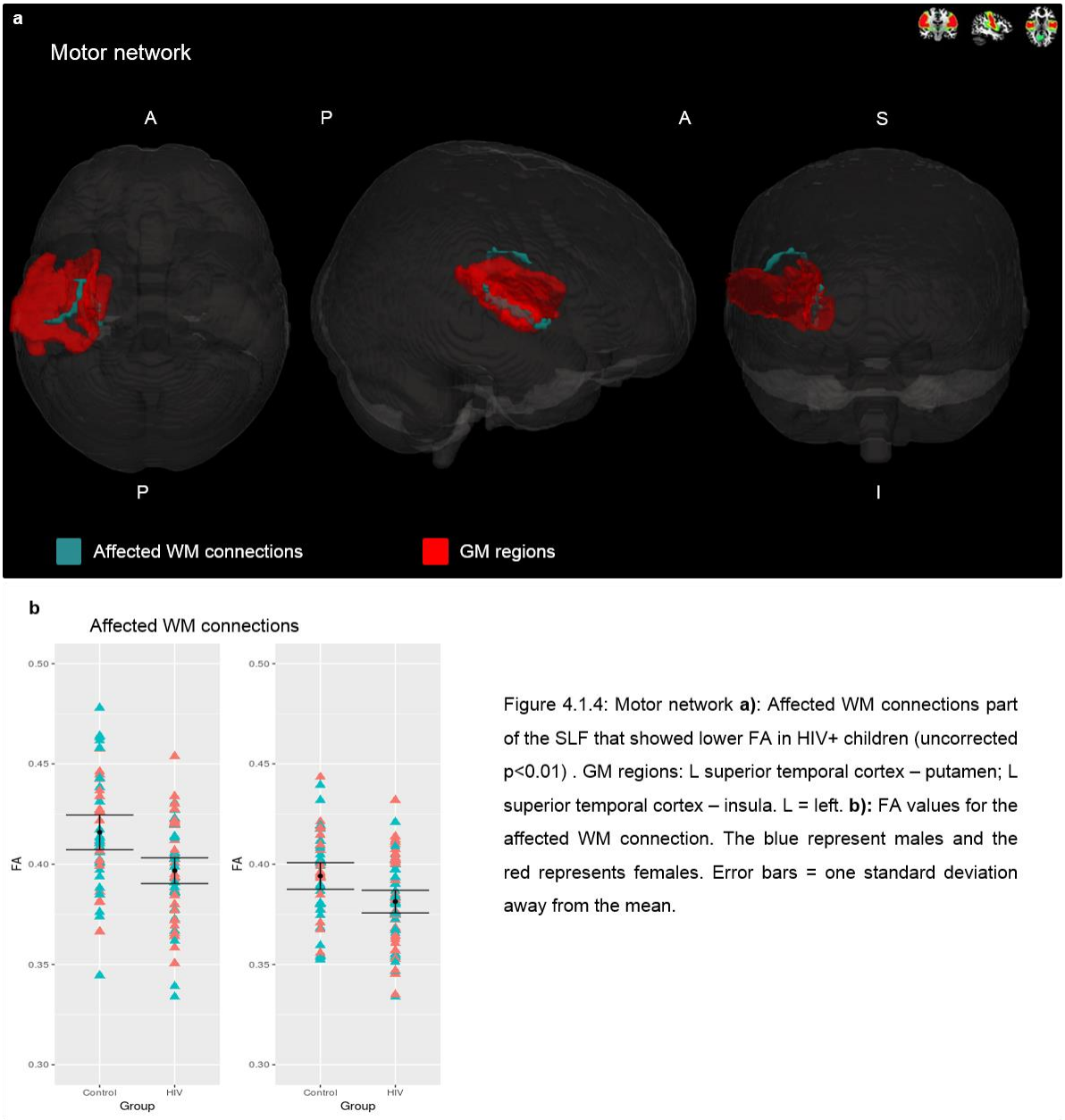

Figure 4.1.4: Motor network **a)**: Affected WM connections part of the SLF that showed lower FA in HIV+ children (uncorrected p<0.01) . GM regions: L superior temporal cortex – putamen; L superior temporal cortex – insula. L = left. **b):** FA values for the affected WM connection. The blue represent males and the red represents females. Error bars = one standard deviation away from the mean.

Table 4.1: Group means (**μ)** and standard deviations (**σ)**, Beta (β), standard error (std error), standardized beta (std β), and p values for FA, AD and RD in tracts that were statistically significant ($p < 0.01$) (HIV+<controls)

Somatosensory network	Controls μ σ	HIV μ σ	β	std error	std β	p value
External capsule (R putamen – superior temporal cortex)						
FA	0.42 0.03	0.41 0.03	-0.0172	0.0065	-0.25	0.010
AD	1.22 0.05	1.22 0.05	-0.0048	0.0094	-0.0492	0.6132
RD	0.62 0.03	0.64 0.03	0.0164	0.0062	0.2548	0.0091
Salience network	**Controls μ σ**	**HIV μ σ**	**β**	**std error**	**std β**	**p value**
WM connections (R lateral orbitofrontal cortex – rostral anterior cingulate cortex)						
FA	0.41 0.05	0.38 0.06	-0.0309	0.0108	-0.2673	0.0051
AD	1.30 0.07	1.29 0.08	-0.0119	0.0153	-0.0761	0.4395
RD	0.66 0.04	0.63 0.06	0.0343	0.0104	0.3025	0.0013
Auditory network	**Controls μ σ**	**HIV μ σ**	**β**	**std error**	**std β**	**p value**
SLF (R inferior parietal cortex – superior temporal cortex)						
FA	0.35 0.02	0.35 0.03	-0.0141	0.0052	-0.2559	0.0082
AD	1.24 0.03	1.26 0.06	-0.0014	0.0088	-0.0154	0.874
RD	0.72 0.03	0.73 0.05	0.0147	0.0067	0.2103	0.0316
Motor network	**Controls μ σ**	**HIV μ σ**	**β**	**std error**	**std β**	**p value**
WM connections (L putamen – superior temporal cortex)						
FA	0.42 0.03	0.40 0.03	-0.0178	0.0057	-0.2953	0.0023
AD	1.22 0.05	1.21 0.05	-0.0121	0.0096	-0.1236	0.2105
RD	0.62	0.64	0.0149	0.0054	0.2616	0.0073

	0.03	0.03				
WM connections (L superior temporal cortex – insula)						
FA	0.39 0.02	0.38 0.02	-0.0131	0.0044	-0.2847	0.0034
AD	1.18 0.05	1.18 0.04	-0.004	0.0082	-0.0481	0.6278
RD	0.63 0.03	0.65 0.02	0.0137	0.0049	0.2643	0.0066

R = right; L = left.

4.2 MD HIV vs Controls

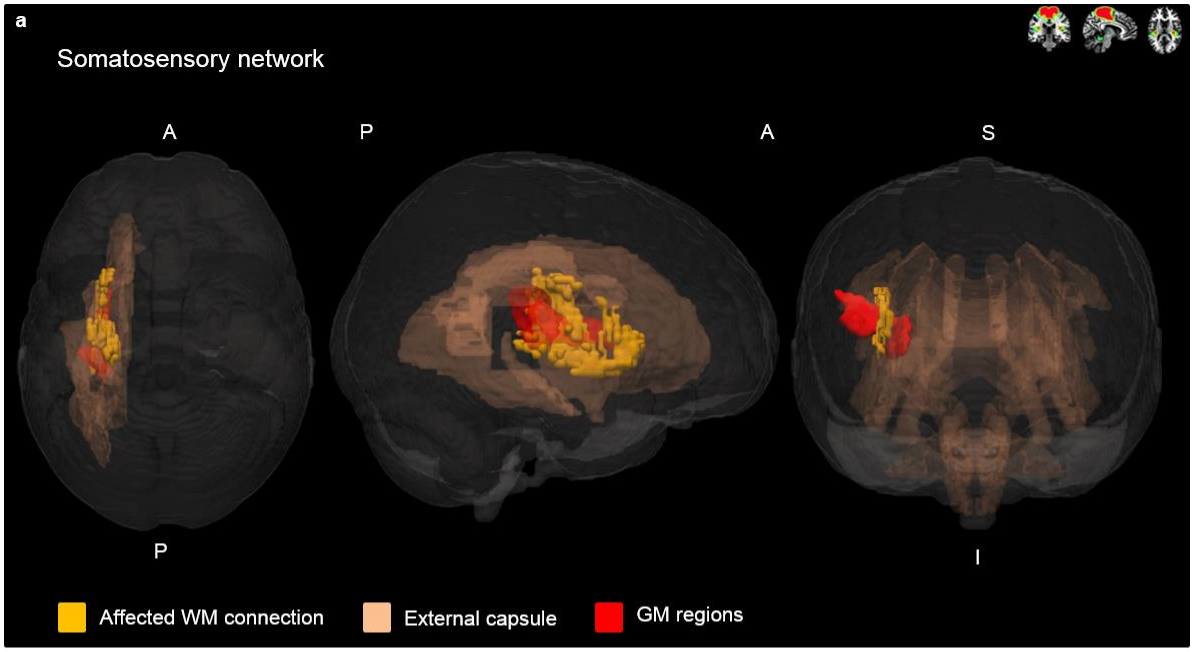

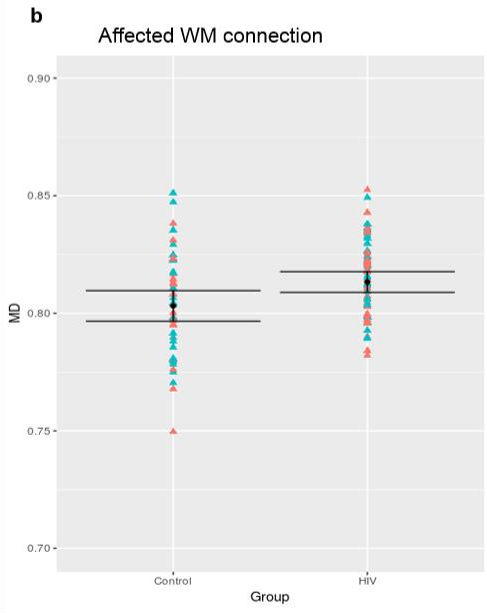

Figure 4.2.1: Somatosensory network **a)**: Affected WM connection part of the external capsule that showed higher MD in HIV+ children (uncorrected p<0.01) . GM regions: L putamen – insula. L = left. **b):** MD values (μm/ms) for the affected WM connection. The blue represent males and the red represents females. Error bars = one standard deviation away from the mean.

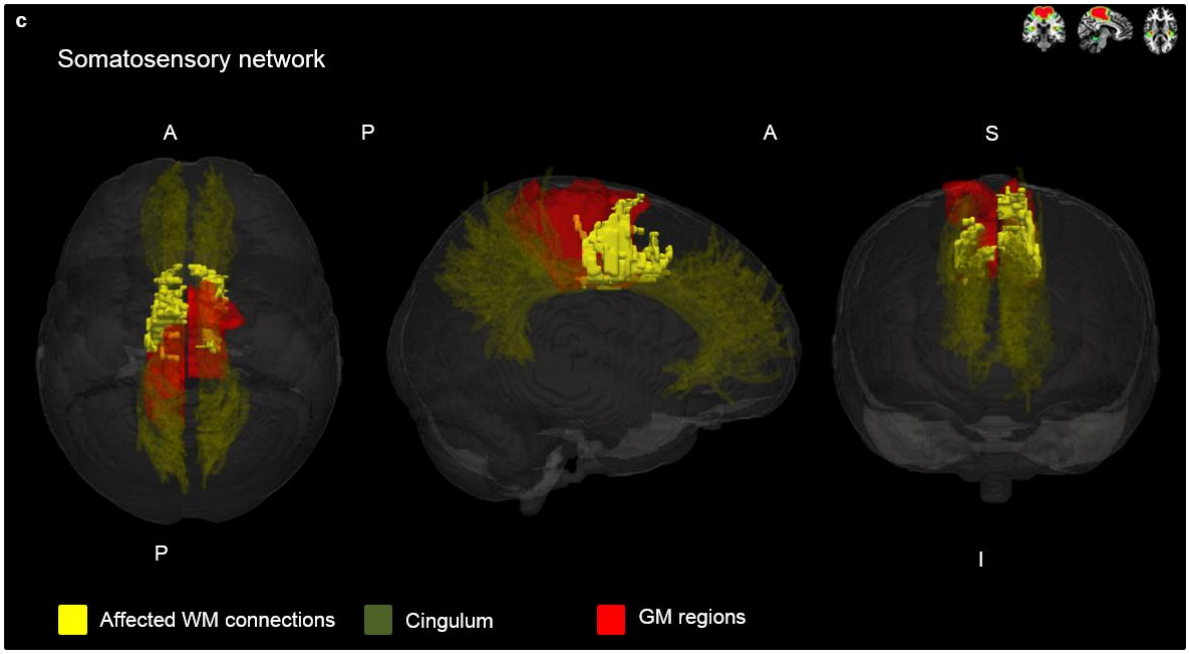

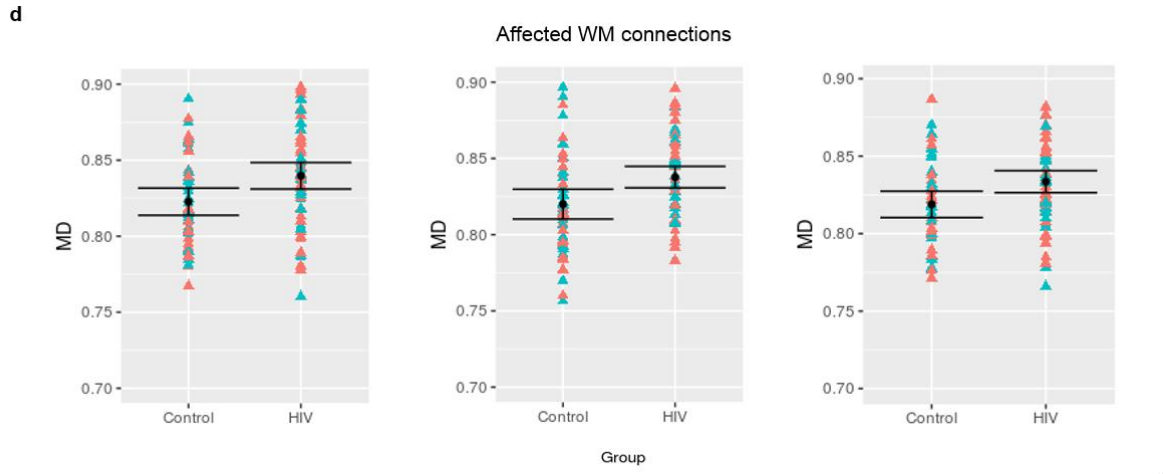

Figure 4.2.1: (*cont'd*) **c)**: Affected WM connections part of the cingulum tract that showed higher MD in HIV+ children (uncorrected p<0.01) . GM regions: L superior frontal cortex – paracentral cortex; superior frontal cortex – posterior cingulate cortex (bilateral). L = left. **d):** MD values (μm/ms) for the affected WM connections. The blue represent males and the red represents females. Error bars = one standard deviation away from the mean.

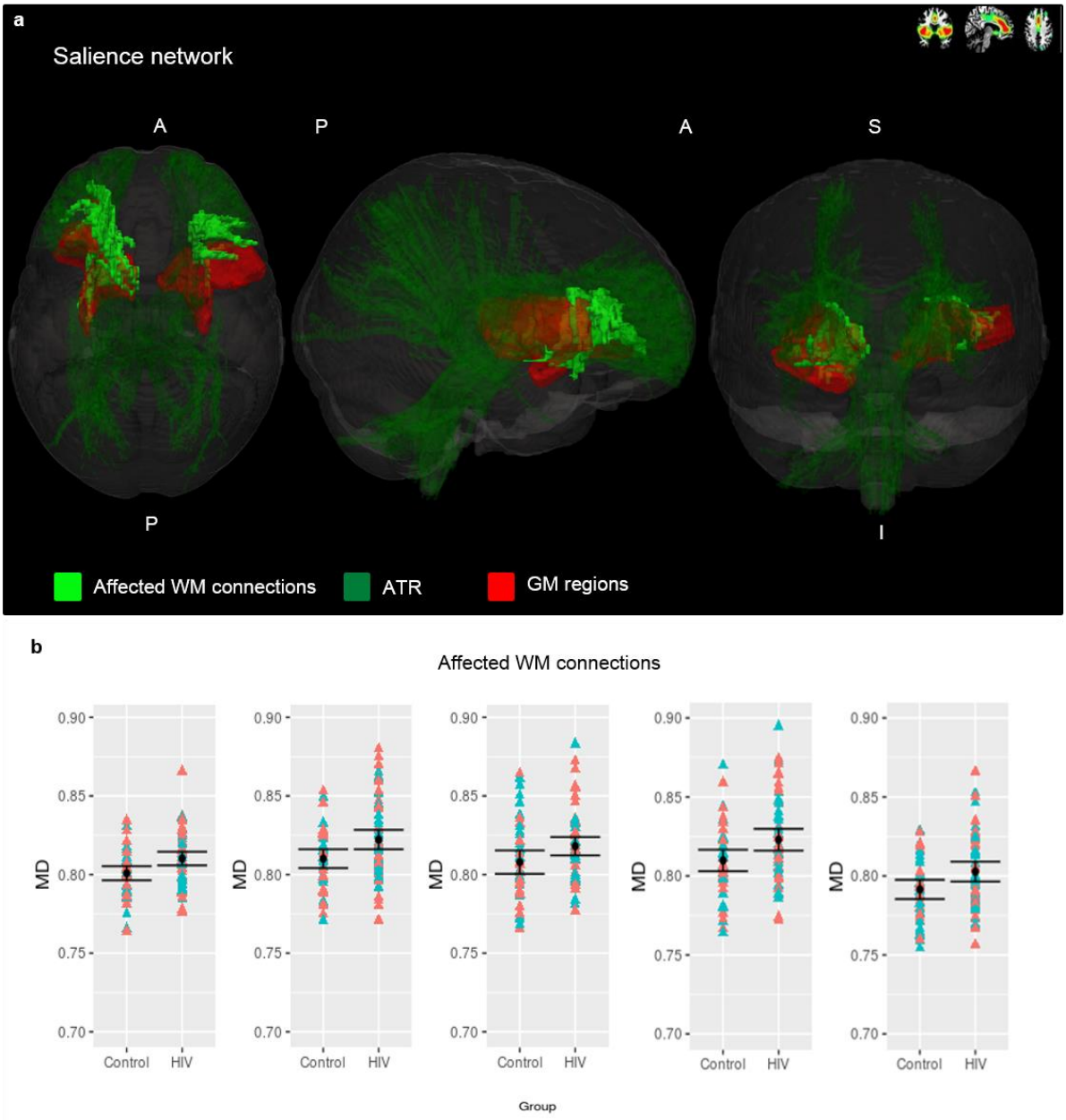

Figure 4.2.2: Salience network **a)**: Affected WM connections part of the ATR that showed higher MD in HIV+ children (uncorrected p<0.01) . GM regions: L caudate – putamen; L caudate – lateral orbitofrontal cortex; L putamen – lateral orbitofrontal cortex; L putamen – parstriangularis; R putamen – parsopercularis. L = left, R = right. **b):** MD values (μm/ms) for the affected WM connections. The blue represent males and the red represents females. Error bars = one standard deviation away from the mean.

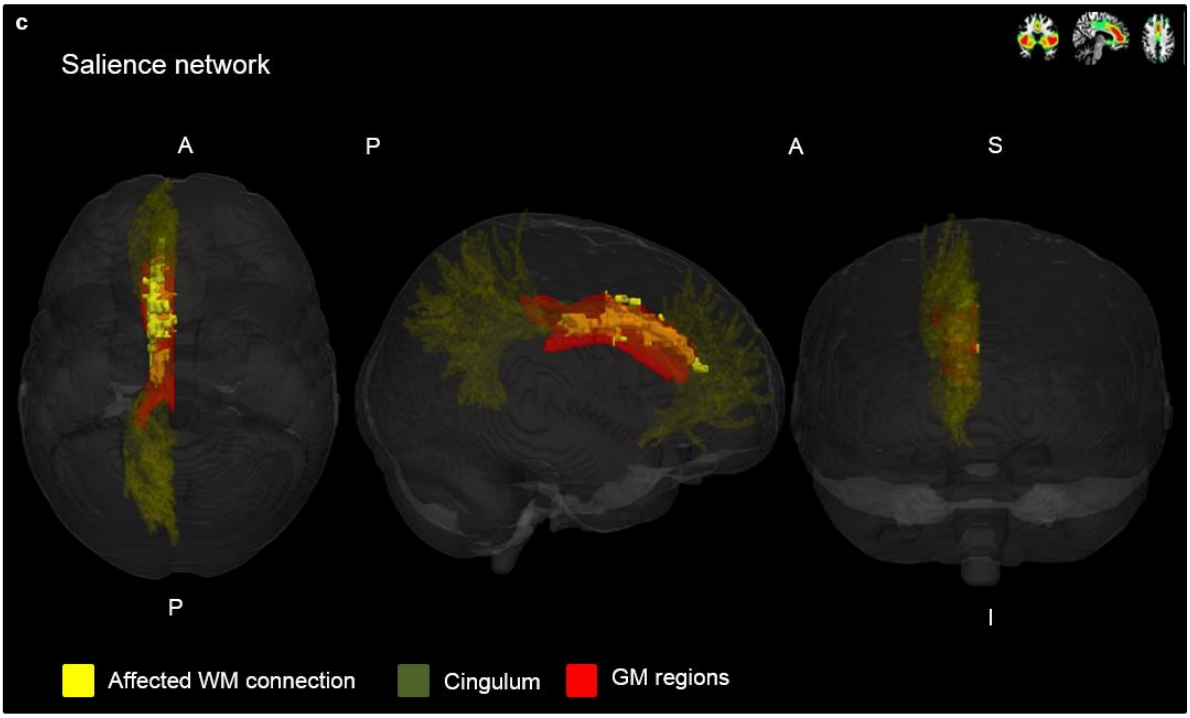

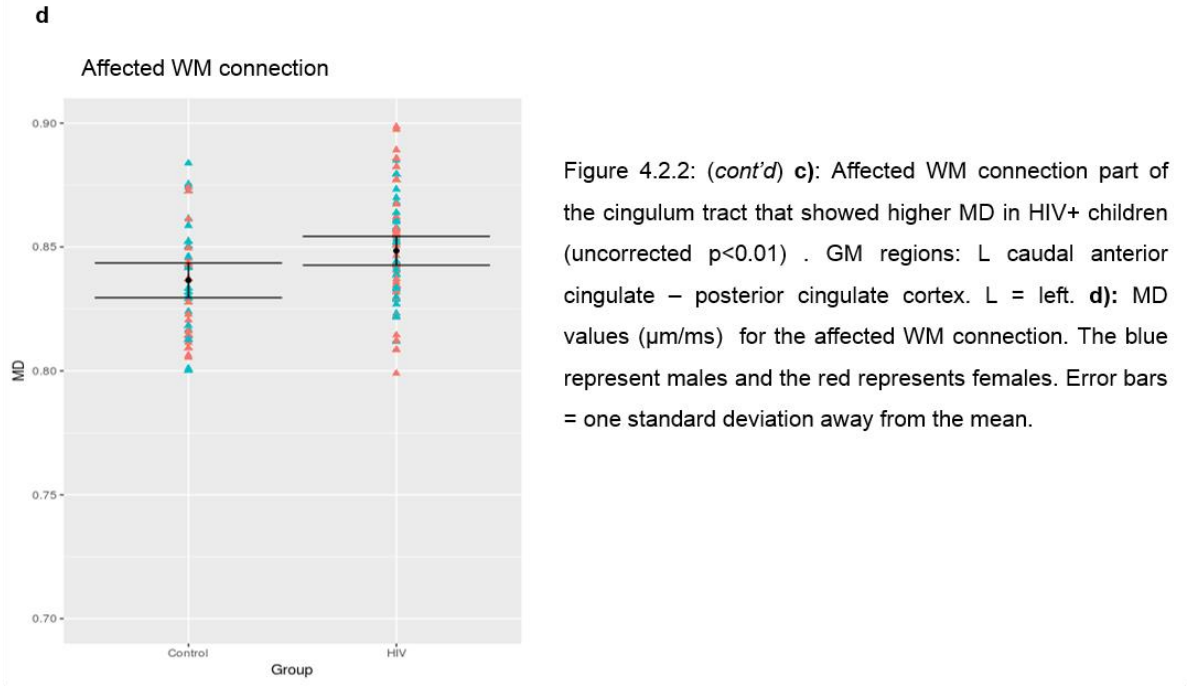

Figure 4.2.2: (*cont'd*) **c)**: Affected WM connection part of the cingulum tract that showed higher MD in HIV+ children (uncorrected p<0.01) . GM regions: L caudal anterior cingulate – posterior cingulate cortex. L = left. **d):** MD values (μm/ms) for the affected WM connection. The blue represent males and the red represents females. Error bars = one standard deviation away from the mean.

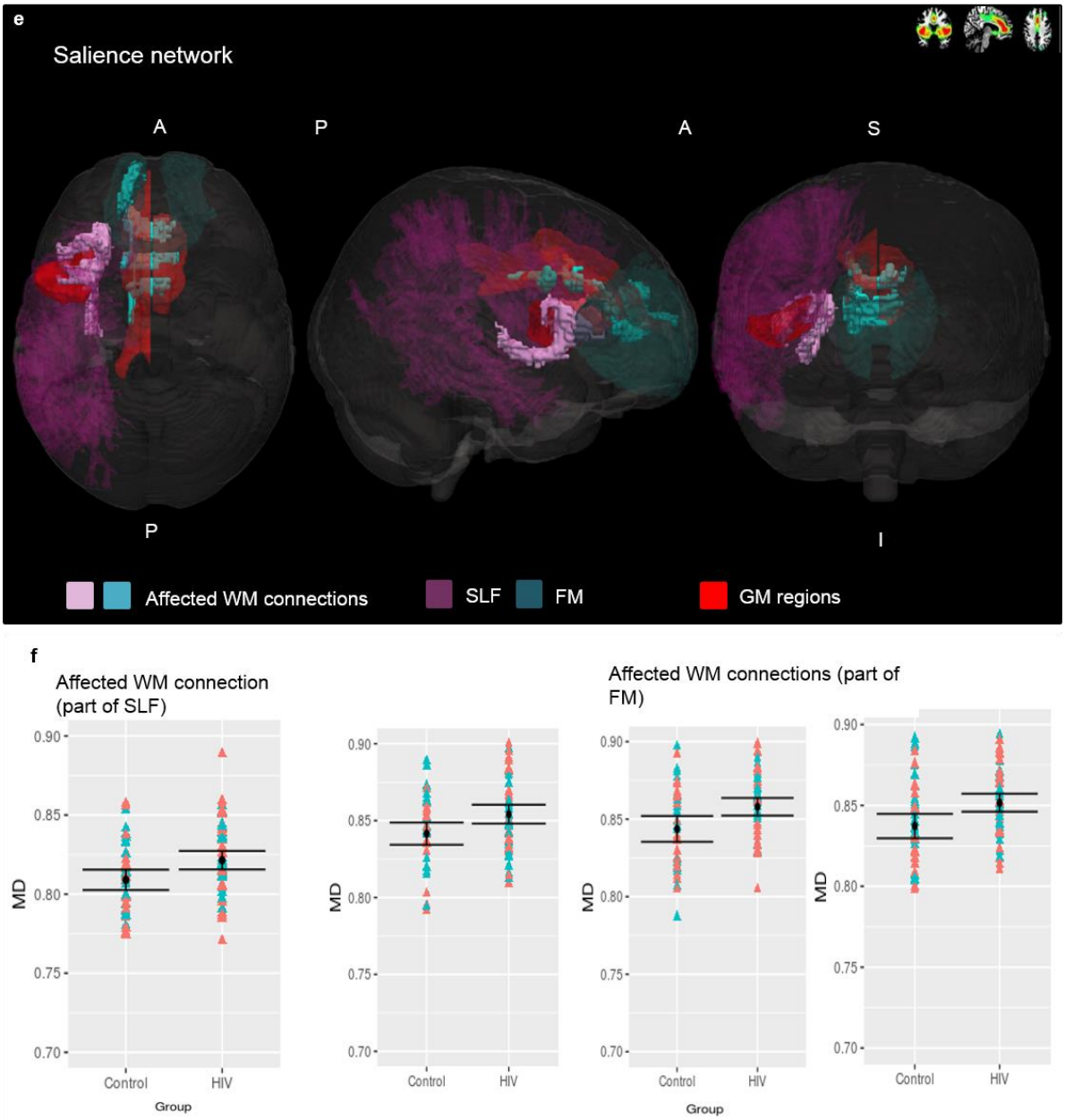

Figure 4.2.2: (*cont'd*) **e)**: Affected WM connections part of the SLF (in purple) and FM (in turquoise) that showed higher MD in HIV+ children (uncorrected p<0.01) . GM regions: connected by SLF: L parsopercularis – insula; connected by FM: R caudal anterior cingulate cortex – L posterior cingulate; L superior frontal cortex - R caudal anterior cingulate cortex; L rostral anterior cingulate cortex – superior frontal cortex. L = left; R = right. **f):** MD values (μm/ms) for the affected WM connections. The blue represent males and the red represents females. Error bars = one standard deviation away from the mean.

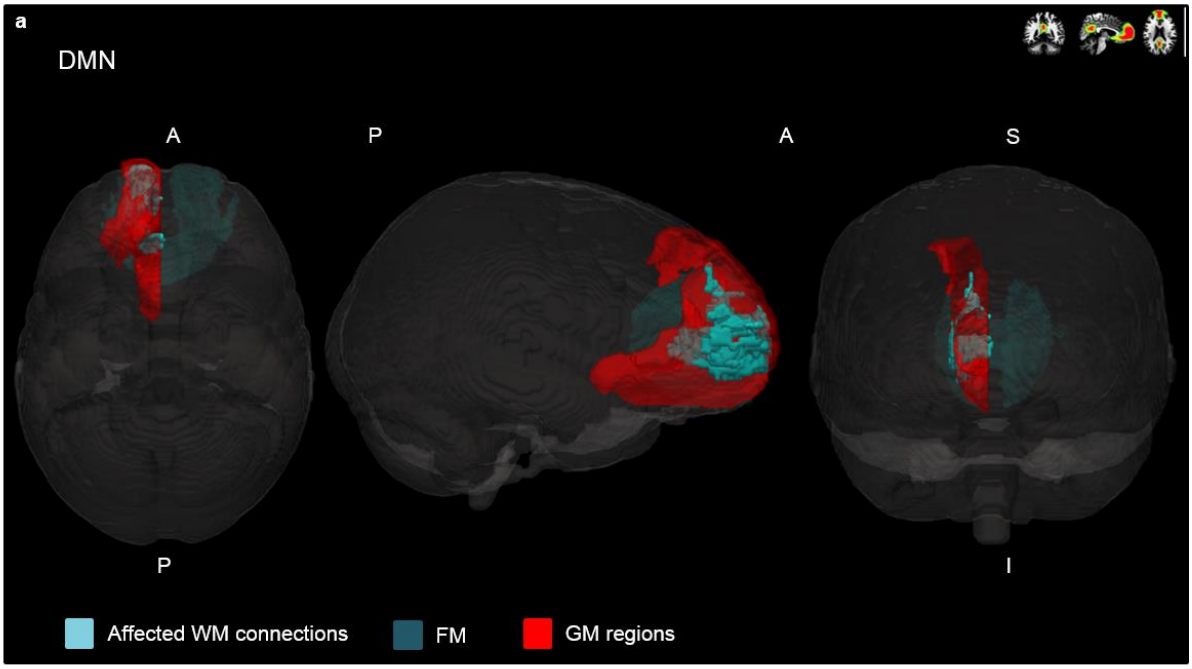

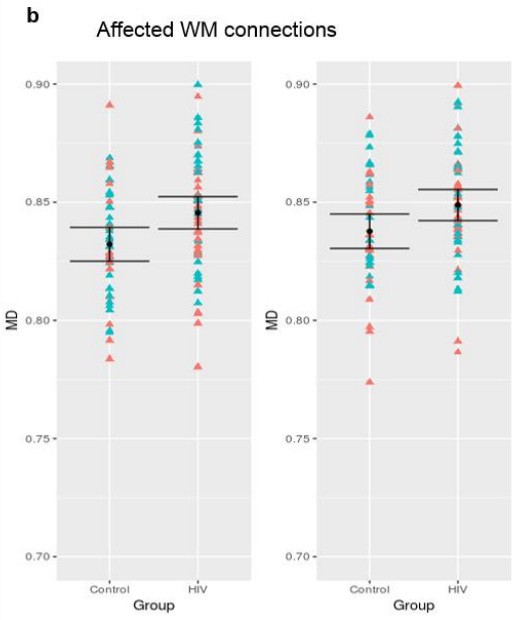

Figure 4.2.3: DMN **a)**: Affected WM connections part of the FM that showed higher MD in HIV+ children (uncorrected p<0.01). GM regions: L superior frontal cortex – medial orbitofrontal cortex; L superior frontal cortex – rostral anterior cingulate cortex. L = left. **b):** MD values (μm/ms) for the affected WM connections. The blue represent males and the red represents females. Error bars = one standard deviation away from the mean.

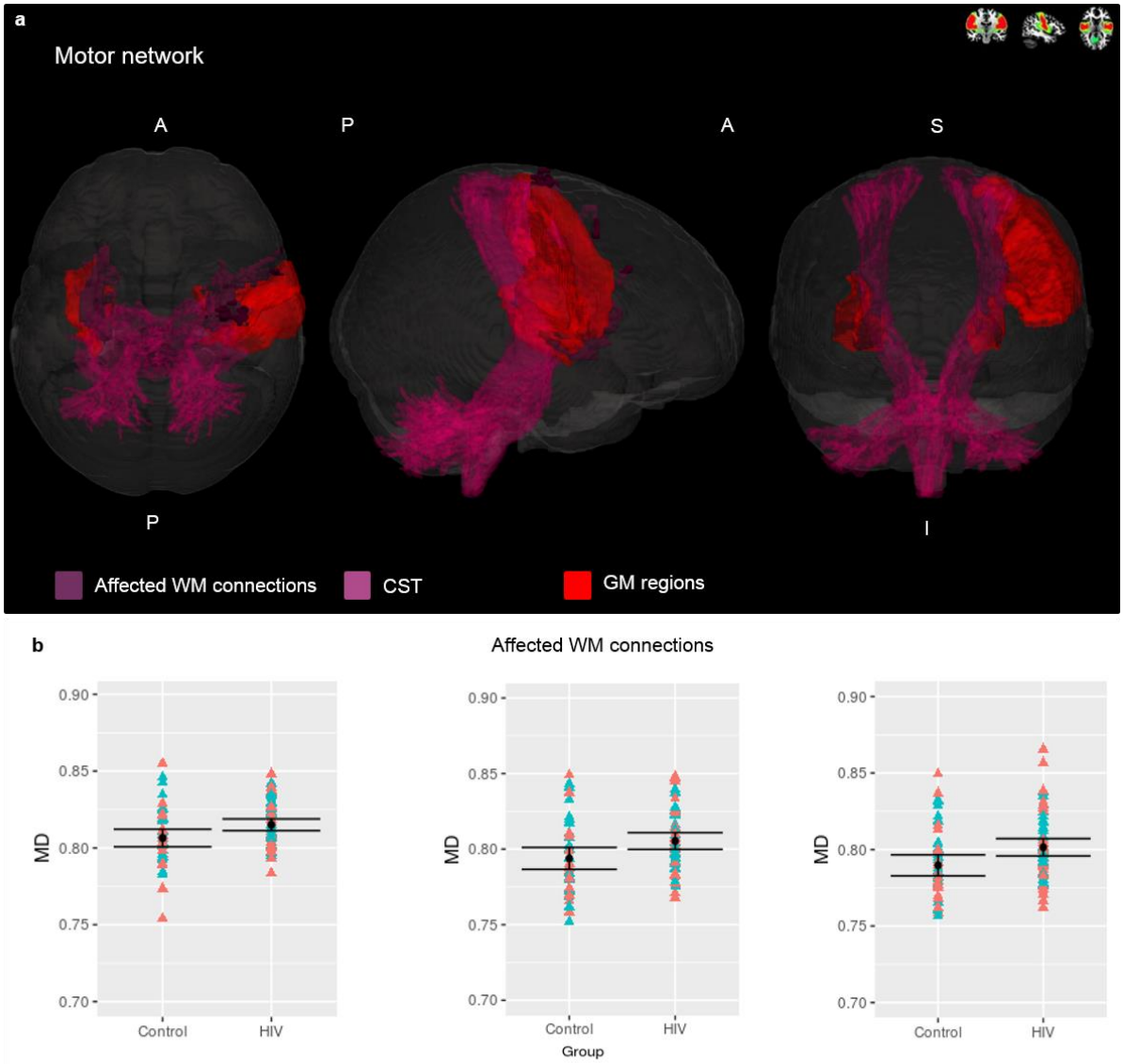

Figure 4.2.4: Motor network **a)**: Affected WM connections part of the CST that showed higher MD in HIV+ children (uncorrected p<0.01) . GM regions: L putamen – insula; R putamen – post central cortex; R putamen – precentral cortex. L = left; R = right. **b):** MD values (μm/ms) for the affected WM connections. The blue represent males and the red represents females. Error bars = one standard deviation away from the mean.

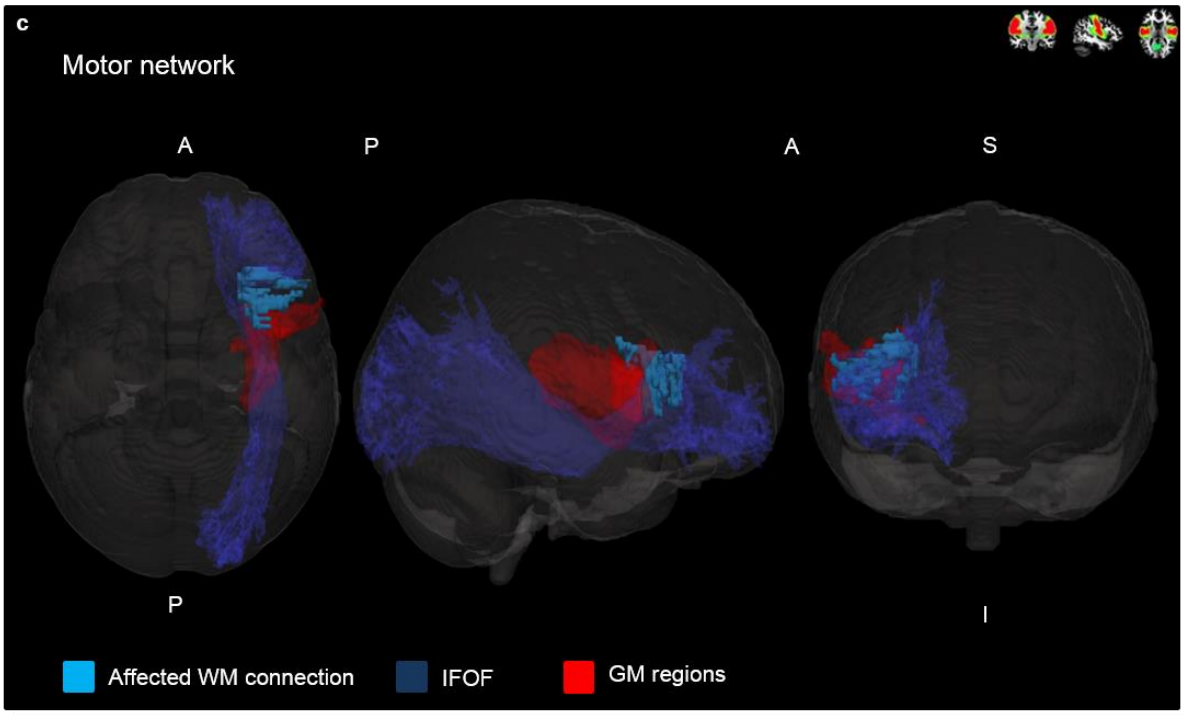

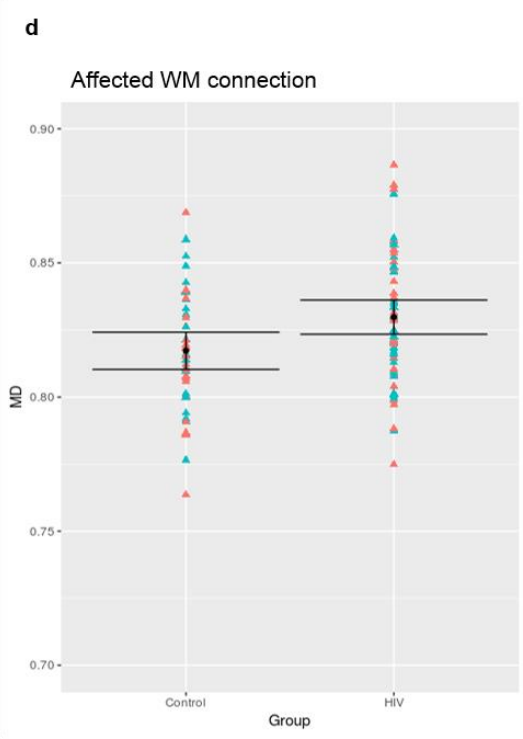

Figure 4.2.4: (*cont'd*) **c)**: Affected WM connection part of the IFOF that showed higher MD in HIV+ children (uncorrected p<0.01) . GM regions: R parsopercularis – insula. R = right. **d):** MD values (μm/ms) for the affected WM connection. The blue represent males and the red represents females. Error bars = one standard deviation away from the mean.

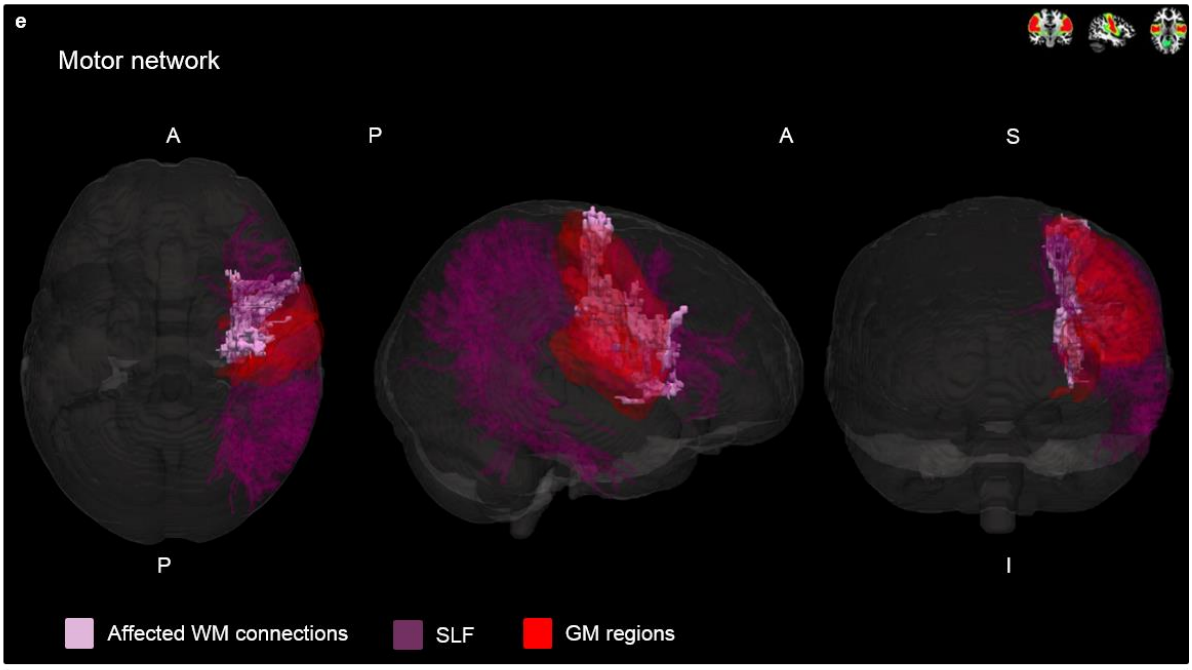

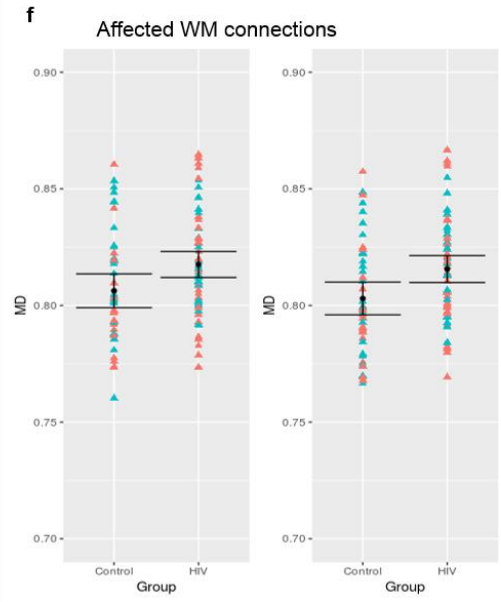

Figure 4.2.4: (*cont'd*) **e)**: Affected WM connections part of the SLF that showed higher MD in HIV+ children (uncorrected p<0.01). GM regions: R insula – postcentral cortex; R insula – precentral cortex. R = right. **f):** MD values (μm/ms) for the affected WM connections. The blue represent males and the red represents females. Error bars = one standard deviation away from the mean.

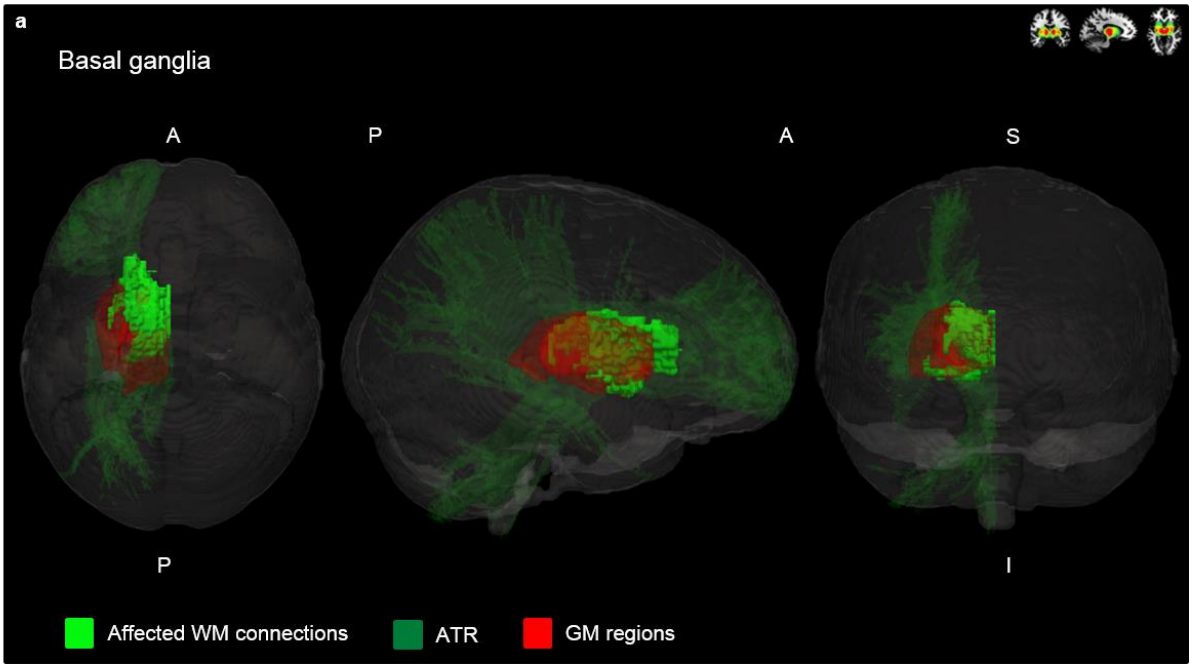

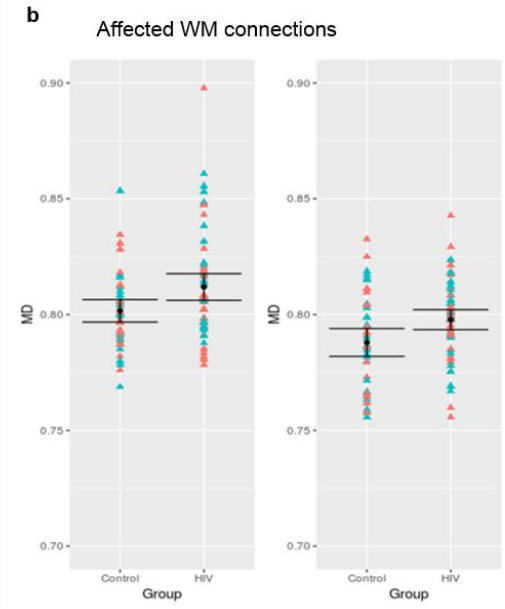

Figure 4.2.5: Basal ganglia **a)**: Affected WM connections part of the ATR that showed higher MD in HIV+ children (uncorrected p<0.01). GM regions: L caudate – thalamus; L caudate – putamen. L =left. **b):** MD values (μm/ms) for the affected WM connections. The blue represent males and the red represents females. Error bars = one standard deviation away from the mean.

Table 4.2: Group means (**μ)** and standard deviations (**σ)**, Beta (β), standard error (std error), standardized beta (std β), and p values for MD, AD and RD in tracts that were statistically significant ($p < 0.01$) (HIV+ >controls)

Somatosensory network	Controls μ σ	HIV μ σ	β	std error	std β	p value
Cingulum*						
(R posterior cingulate cortex – superior frontal cortex)						
MD	0.82 0.03	0.84 0.03	0.0205	0.0062	0.3112	0.0012
AD	1.19 0.05	1.21 0.04	0.0225	0.0094	0.2281	0.0189
RD	0.64 0.03	0.66 0.03	0.0195	0.0073	0.2844	0.0034
Cingulum						
(L paracentral gyrus – superior frontal cortex)						
MD	0.82 0.03	0.84 0.03	0.0186	0.0064	0.2748	0.0045
AD	1.18 0.05	1.20 0.05	0.021	0.0103	0.1981	0.0437
RD	0.64 0.03	0.66 0.03	0.0192	0.0065	0.254	0.0082
Cingulum						
(L putamen – insula)						
MD	0.80 0.02	0.81 0.02	0.0104	0.0038	0.2596	0.0077
AD	1.20 0.04	1.21 0.03	0.0099	0.0061	0.1583	0.1063
RD	0.61 0.02	0.62 0.02	0.0106	0.0043	0.254	0.0151
Cingulum						
(L posterior cingulate cortex – superior frontal cortex)						
MD	0.82 0.03	0.83 0.03	0.0162	0.0057	0.2722	0.005
AD	1.20 0.05	1.21 0.05	0.0159	0.0093	0.1652	0.0908
RD	0.63 0.03	0.65 0.03	0.0163	0.006	0.2555	0.0073
Salience network	Controls μ σ	HIV μ σ	β	std error	std β	p value
ATR*						
(L caudate – putamen)						
MD	0.80 0.02	0.81 0.02	0.0092	0.0032	0.2725	0.005
AD	1.16 0.03	1.17 0.02	0.0085	0.0052	0.1615	0.1007
RD	0.62	0.63	0.0095	0.004	0.2302	0.0185

	0.02	0.02				
ATR*						
(L caudate – lateral orbitofrontal cortex)						
MD	0.81 0.02	0.82 0.03	0.0143	0.0052	0.2645	0.0066
AD	1.20 0.03	1.21 0.04	0.0101	0.0066	0.1488	0.1288
RD	0.62 0.03	0.63 0.03	0.0165	0.0062	0.2537	0.0088
ATR*						
(L putamen – lateral orbitofrontal cortex)						
MD	0.81 0.02	0.82 0.02	0.0123	0.0044	0.2641	0.0065
AD	1.18 0.03	1.19 0.03	0.0111	0.006	0.179	0.068
RD	0.62 0.02	0.64 0.03	0.0129	0.0051	0.2395	0.0139
ATR*						
(L putamen – parstriangularis)						
MD	0.79 0.02	0.80 0.02	0.0113	0.0045	0.2396	0.0143
AD	1.17 0.03	1.18 0.03	0.0089	0.0062	0.1394	0.1538
RD	0.60 0.02	0.61 0.03	0.0125	0.0054	0.2216	0.0232
ATR*						
(R putamen – parsopercularis)						
MD	0.81 0.03	0.82 0.03	0.013	0.0051	0.2394	0.0135
AD	1.17 0.05	1.18 0.03	0.0106	0.0078	0.133	0.1765
RD	0.63 0.02	0.64 0.03	0.0141	0.0055	0.2443	0.0115
Cingulum*						
(L caudal anterior cingulate cortex – posterior cingulate cortex)						
MD	0.84 0.02	0.85 0.02	0.0132	0.0046	0.2712	0.0052
AD	1.24 0.04	1.26 0.03	0.0179	0.0065	0.2576	0.0069
RD	0.63 0.03	0.64 0.03	0.0108	0.0052	0.1986	0.0408
SLF*						
(L parsopercularis – insula)						
MD	0.86 0.02	0.87 0.02	0.0125	0.0044	0.2698	0.0055
AD	1.18 0.04	1.19 0.03	0.0121	0.0059	0.1996	0.0418
RD	0.62 0.02	0.63 0.03	0.0127	0.0047	0.2582	0.0081
FM*						
(L superior frontal cortex – R caudal anterior cingulate cortex)						
MD	0.84 0.03	0.86 0.03	0.0186	0.0075	0.2386	0.0147

AD	1.38 0.04	1.39 0.03	0.0465	0.0139	0.3141	0.0011
RD	0.57 0.03	0.59 0.03	0.0046	0.0088	0.0518	0.6
Cingulum*						
(L posterior cingulate cortex – R caudal anterior cingulate cortex)						
MD	0.85 0.04	0.87 0.04	0.0123	0.005	0.2384	0.0148
AD	1.43 0.07	1.48 0.07	0.012	0.0067	0.1706	0.0769
RD	0.56 0.04	0.57 0.05	0.0124	0.0058	0.2073	0.0333
Cingulum*						
(R caudal anterior cingulate cortex – posterior cingulate cortex)						
MD	0.84 0.03	0.86 0.03	0.0179	0.0051	0.3293	0.0006
AD	1.23 0.04	1.25 0.04	0.0239	0.0084	0.2711	0.0053
RD	0.64 0.03	0.66 0.03	0.0149	0.0054	0.2623	0.0063
DMN						
	Controls μ σ	HIV μ σ	β	std error	std β	p value
FM*						
(L medial orbitofrontal cortex – superior frontal cortex)						
MD	0.83 0.02	0.85 0.03	0.0161	0.0051	0.2928	0.0023
AD	1.20 0.07	1.21 0.06	0.0102	0.0125	0.0801	0.4145
RD	0.65 0.04	0.67 0.04	0.0191	0.0074	0.2473	0.0113
FM*						
(L rostral anterior cingulate – superior frontal cortex)						
MD	0.84 0.02	0.85 0.03	0.0148	0.0051	0.274	0.0043
AD	1.26 0.05	1.27 0.05	0.0161	0.0096	0.1608	0.0972
RD	0.63 0.03	0.64 0.03	0.0142	0.0065	0.2093	0.0326
Basal ganglia						
	Controls μ σ	HIV μ σ	β	std error	std β	p value
ATR						
(L thalamus proper – caudate)						
MD	0.80 0.02	0.81 0.02	0.0104	0.004	0.2522	0.0097
AD	1.14 0.03	1.15 0.03	0.0141	0.0054	0.2482	0.0096
RD	0.63 0.02	0.64 0.03	0.0086	0.0047	0.1787	0.0678
ATR						
(L caudate – putamen)						
MD	0.79 0.02	0.80 0.02	0.0096	0.0036	0.2528	0.0093

AD	1.19 0.03	1.20 0.03	0.0085	0.0061	0.1353	0.1672
RD	0.59 0.02	0.60 0.02	0.0101	0.0048	0.202	0.0362
Motor network						
	Controls μ σ	HIV μ σ	β	std error	std β	p value
WM connections (L putamen – insula)						
MD	0.81 0.02	0.82 0.01	0.0091	0.0033	0.2603	0.0072
AD	1.16 0.03	1.17 0.02	0.0101	0.0053	0.1839	0.0616
RD	0.63 0.02	0.64 0.02	0.0086	0.0036	0.2284	0.0182
WM connections (R putamen – postcentral gyrus)						
MD	0.79 0.02	0.81 0.02	0.012	0.0045	0.2545	0.0089
AD	1.16 0.04	1.17 0.03	0.0086	0.0066	0.1236	0.0616
RD	0.61 0.02	0.62 0.02	0.0137	0.0048	0.2685	0.0055
CST (R putamen – precentral gyrus)						
MD	0.79 0.02	0.80 0.02	0.0119	0.0045	0.2558	0.0087
AD	1.18 0.03	1.19 0.03	0.0108	0.0066	0.1579	0.0616
RD	0.59 0.02	0.61 0.02	0.0125	0.0046	0.259	0.0078
IFOF (R parsopercularis – insula)						
MD	0.82 0.02	0.83 0.02	0.013	0.0048	0.2601	0.0075
AD	1.16 0.03	1.17 0.03	0.0136	0.0066	0.198	0.0425
RD	0.65 0.02	0.66 0.03	0.0127	0.0049	0.249	0.0107
SLF (R postcentral gyrus – insula)						
MD	0.81 0.02	0.82 0.02	0.0119	0.0045	0.2522	0.0092
AD	1.15 0.04	1.16 0.03	0.0162	0.0069	0.2256	0.0198
RD	0.64 0.02	0.65 0.02	0.0098	0.0047	0.2018	0.0388
WM connections (R precentral gyrus – insula)						
MD	0.80 0.02	0.82 0.02	0.0128	0.0045	0.2688	0.0056
AD	1.16 0.04	1.18 0.04	0.0149	0.0073	0.196	0.0449
RD	0.62 0.02	0.64 0.02	0.0118	0.0045	0.2514	0.0098

*survived FDR multiple comparisons correction $p < 0.05$. R = right; L = left.

4.3 FA HEU vs HUU

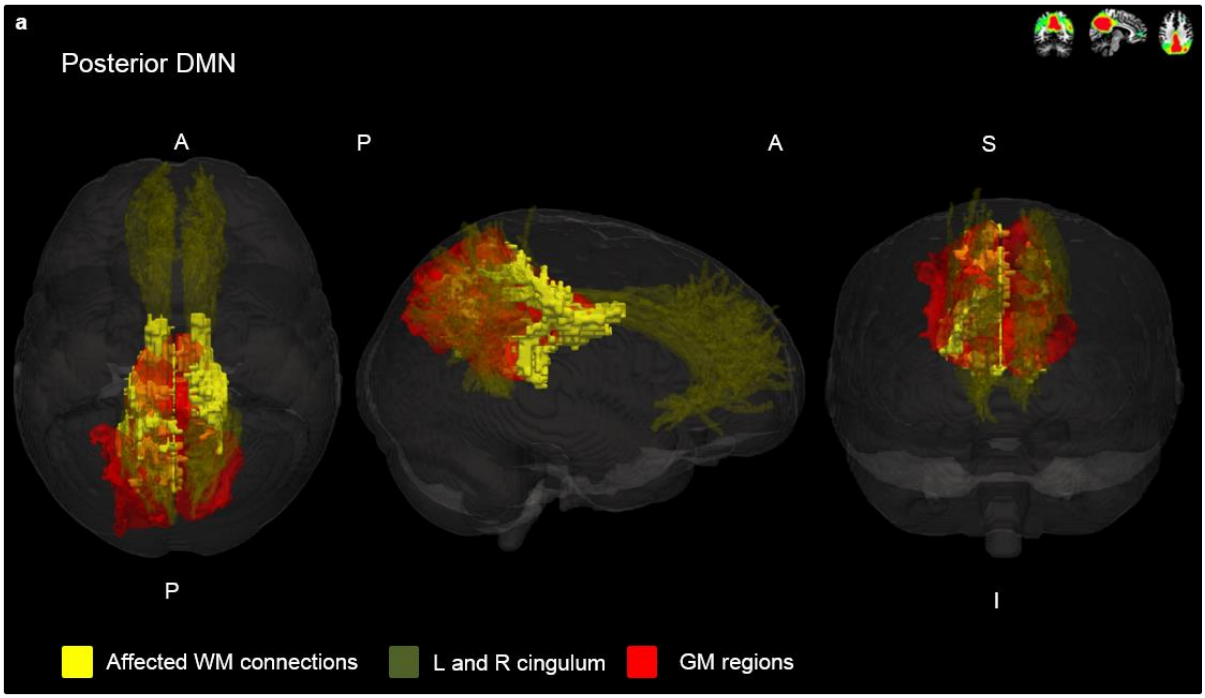

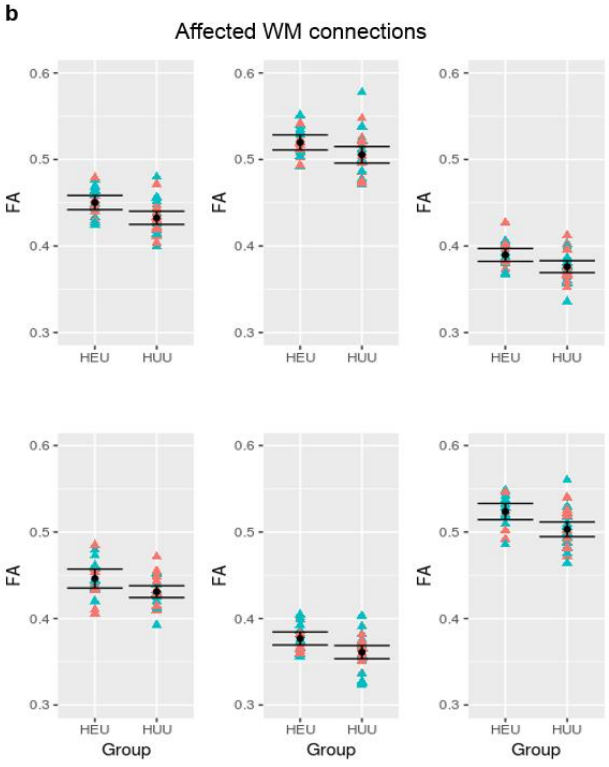

Figure 4.3.1: Posterior DMN **a)**: Affected WM connections part of the cingulum that showed **higher** FA in HEU children (uncorrected p<0.01). GM regions: isthmusingulate – posterior cingulate cortex (bilateral); L isthmuscingulate – precuneus; L paracentral cortex – precuneus; L precuneus – superior parietal cortex; R posterior cingulate cortex – precuneus. L = left, R = right. **b):** FA values for the affected WM connections. The blue represent males and the red represents females. Error bars = one standard deviation away from the mean.

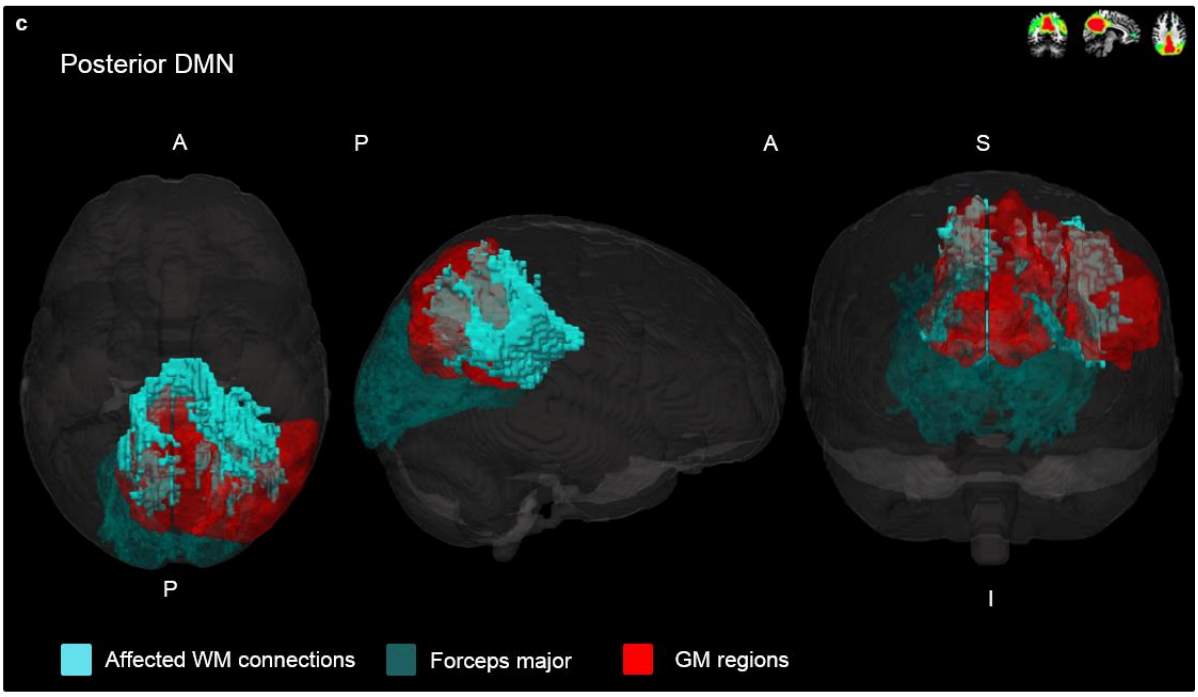

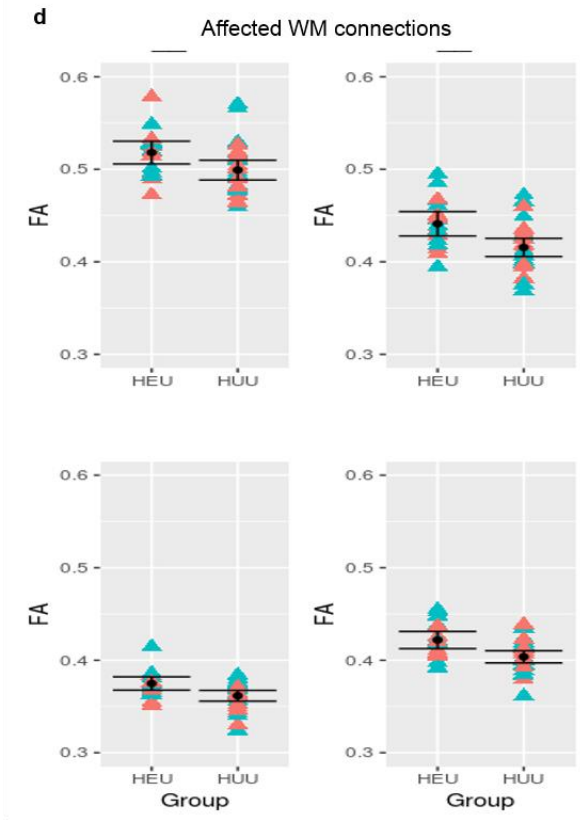

Figure 4.3.1: (*cont'd*) **c)**: Affected WM connections part of the forceps major that showed **higher** FA in HEU children (uncorrected p<0.01). GM regions: L isthmusingulate – R precuneus; L precuneus – R isthmuscingulate; L precuneus – R precuneus; R inferior parietal cortex – superior parietal cortex. L = left, R = right. **d):** FA values for the affected WM connections. The blue represent males and the red represents females. Error bars = one standard deviation away from the mean.

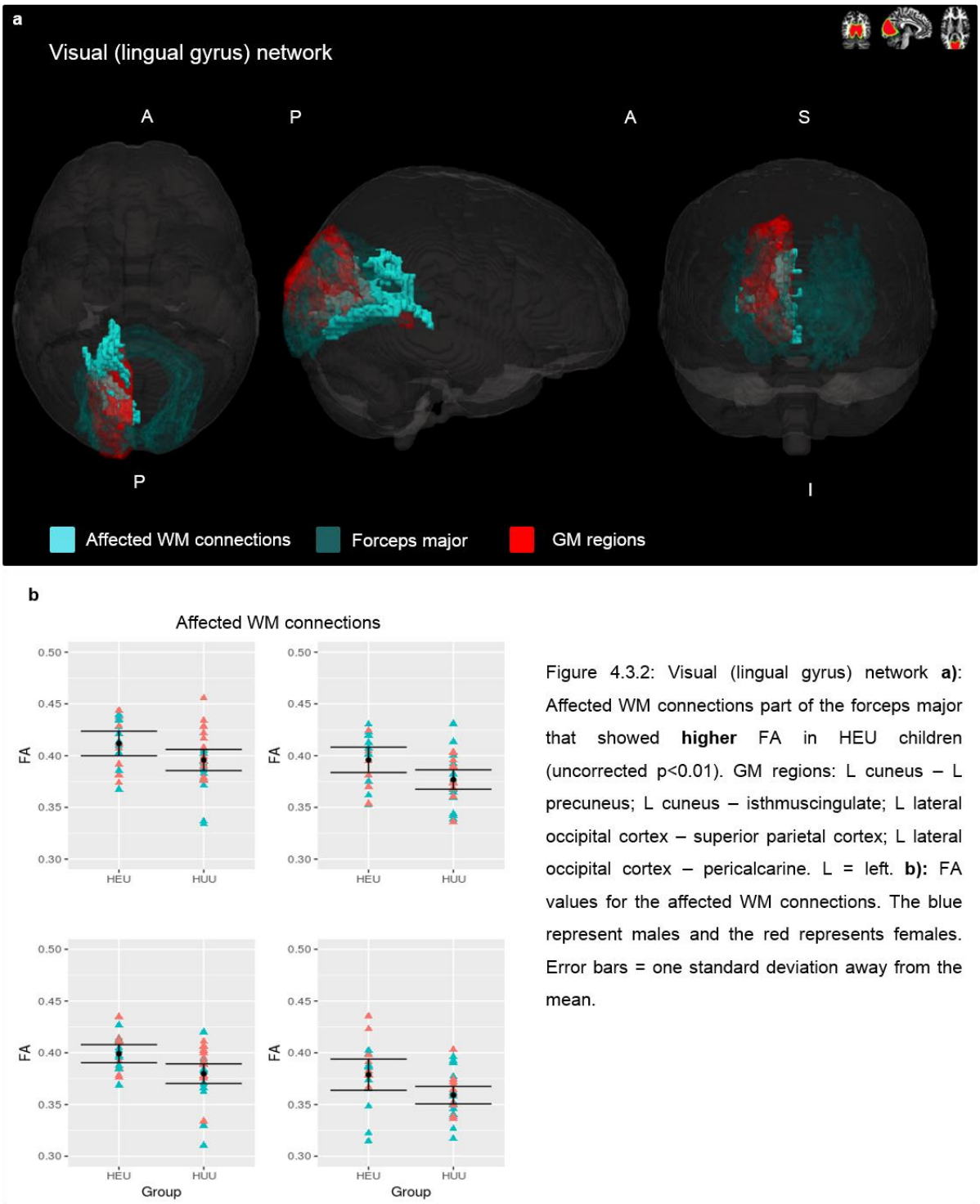

Figure 4.3.2: Visual (lingual gyrus) network **a)**: Affected WM connections part of the forceps major that showed **higher** FA in HEU children (uncorrected p<0.01). GM regions: L cuneus – L precuneus; L cuneus – isthmuscingulate; L lateral occipital cortex – superior parietal cortex; L lateral occipital cortex – pericalcarine. L = left. **b):** FA values for the affected WM connections. The blue represent males and the red represents females. Error bars = one standard deviation away from the mean.

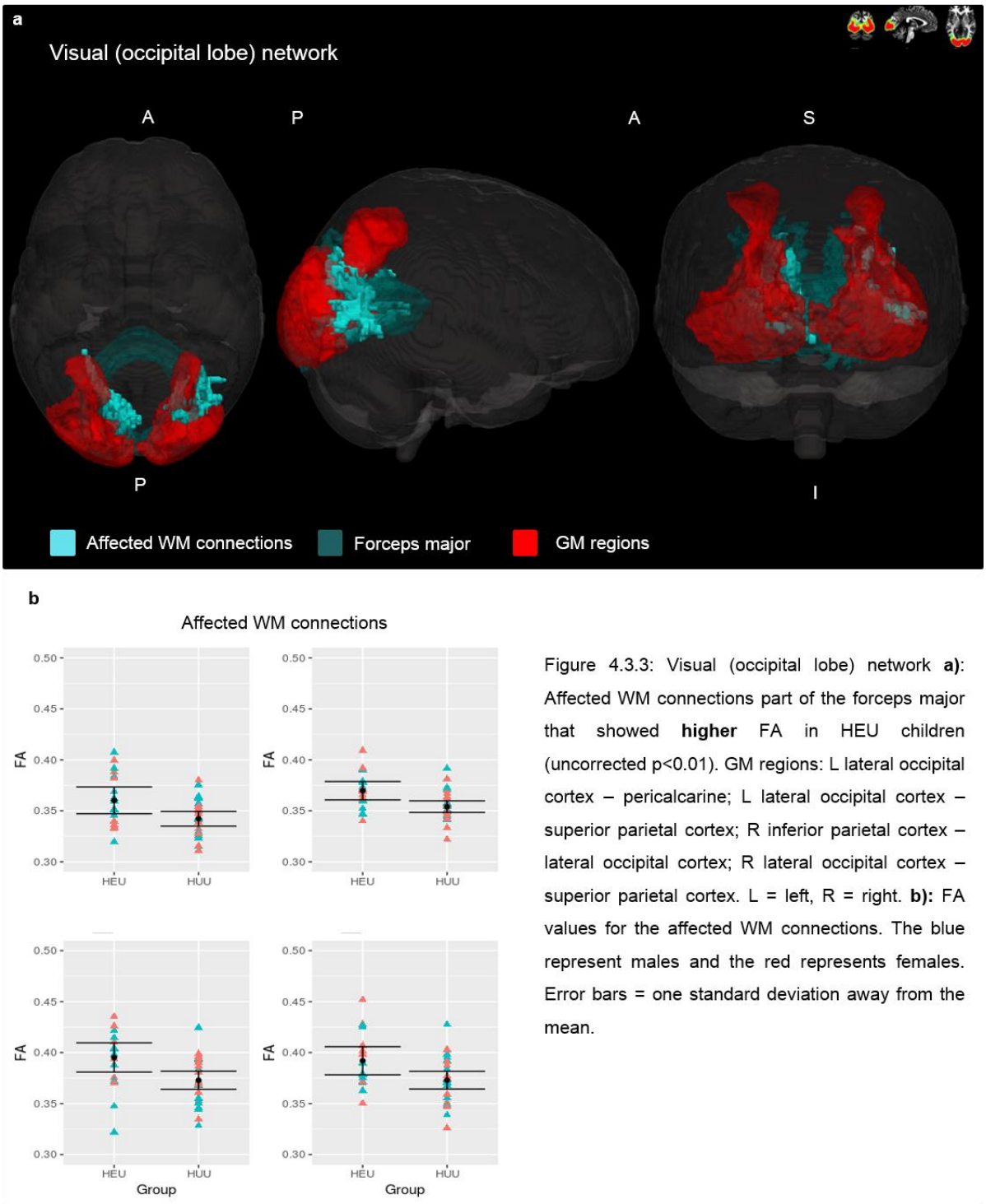

Figure 4.3.3: Visual (occipital lobe) network **a)**: Affected WM connections part of the forceps major that showed **higher** FA in HEU children (uncorrected p<0.01). GM regions: L lateral occipital cortex – pericalcarine; L lateral occipital cortex – superior parietal cortex; R inferior parietal cortex – lateral occipital cortex; R lateral occipital cortex – superior parietal cortex. L = left, R = right. **b):** FA values for the affected WM connections. The blue represent males and the red represents females. Error bars = one standard deviation away from the mean.

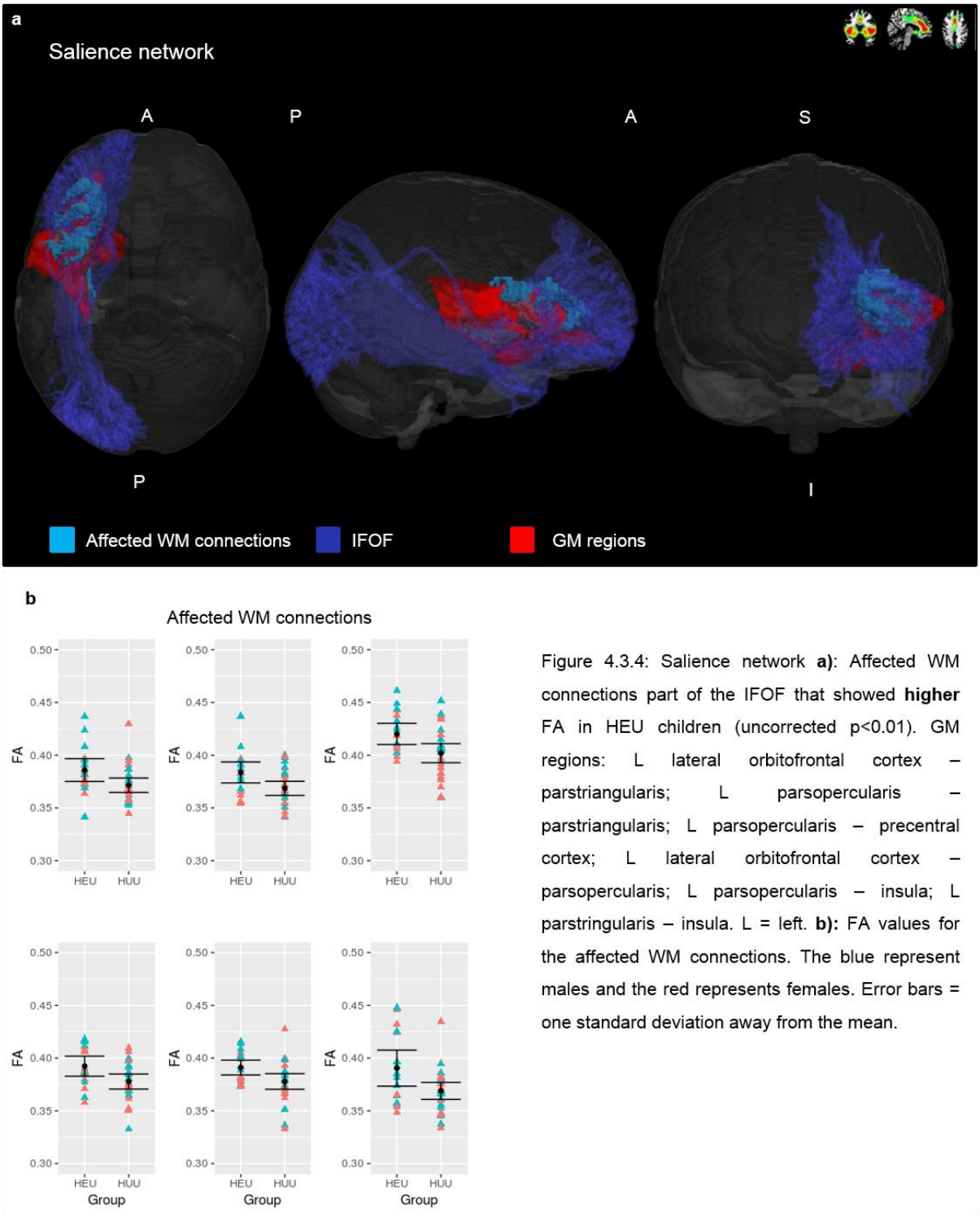

Figure 4.3.4: Salience network **a)**: Affected WM connections part of the IFOF that showed **higher** FA in HEU children (uncorrected p<0.01). GM regions: L lateral orbitofrontal cortex – parstriangularis; L parsopercularis – parstriangularis; L parsopercularis – precentral cortex; L lateral orbitofrontal cortex – parsopercularis; L parsopercularis – insula; L parstringularis – insula. L = left. **b):** FA values for the affected WM connections. The blue represent males and the red represents females. Error bars = one standard deviation away from the mean.

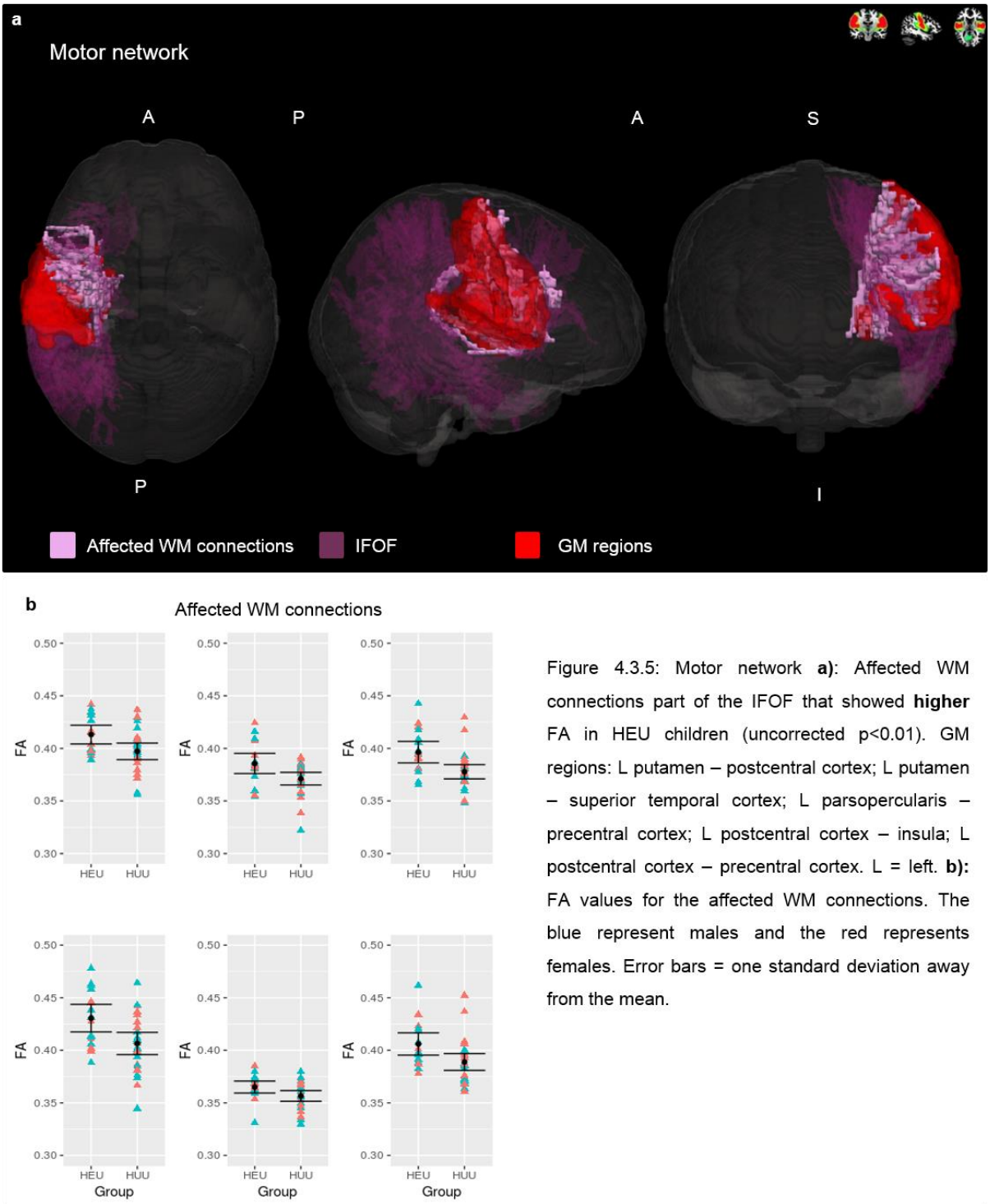

Figure 4.3.5: Motor network **a)**: Affected WM connections part of the IFOF that showed **higher** FA in HEU children (uncorrected p<0.01). GM regions: L putamen – postcentral cortex; L putamen – superior temporal cortex; L parsopercularis – precentral cortex; L postcentral cortex – insula; L postcentral cortex – precentral cortex. L = left. **b):** FA values for the affected WM connections. The blue represent males and the red represents females. Error bars = one standard deviation away from the mean.

Table 4.3: Group means (**μ)** and standard deviations (**σ)**, Beta (β), standard error (std error), standardized beta (std β), and p values for FA, AD and RD in tracts that were statistically significant ($p < 0.01$) (HEU > HUU)

	HEU μ σ	HUU μ σ	β	std error	std β	p value
Posterior DMN						
Cingulum*						
(L isthmuscingulate – posterior cingulate cortex)						
FA	0.45 0.02	0.43 0.02	-0.0179	0.0059	-0.4364	0.0044
AD	1.36 0.05	1.34 0.06	-0.0211	0.0186	-0.18	0.2623
RD	0.63 0.03	0.64 0.03	0.0117	0.0107	0.1744	0.2764
Cingulum*						
(L isthmuscingulate – precuneus)						
FA	0.45 0.02	0.43 0.02	-0.0181	0.0061	-0.4337	0.0047
AD	1.32 0.06	1.32 0.05	0.0013	0.0177	0.0115	0.943
RD	0.62 0.03	0.64 0.04	0.0228	0.0104	0.3327	0.034
Cingulum*						
(L isthmuscingulate – R precuneus)						
FA	0.52 0.02	0.51 0.02	-0.0196	0.0066	-0.418	0.0049
AD	1.44 0.05	1.44 0.06	-0.0075	0.0179	-0.0651	0.6794
RD	0.57 0.03	0.59 0.04	0.0253	0.0114	0.3341	0.0327
Cingulum*						
(L paracentral gyrus – precuneus)						
FA	0.38 0.02	0.36 0.02	-0.0169	0.0058	-0.4271	0.0058
AD	1.21 0.06	1.21 0.05	0.0021	0.0164	0.0202	0.8984
RD	0.66 0.03	0.69 0.04	0.0255	0.0112	0.3417	0.0285
Cingulum*						
(L precuneus – superior parietal cortex)						
FA	0.39 0.01	0.38 0.02	-0.0166	0.0051	-0.4601	0.0024
AD	1.22 0.05	1.22 0.05	0.0054	0.0164	0.0517	0.7454
RD	0.66 0.04	0.68 0.04	0.0246	0.0125	0.2944	0.0564
Cingulum*						

(L precuneus – R isthmuscingulate)						
FA	0.53 0.03	0.50 0.02	-0.0314	0.0086	-0.509	0.0007
AD	1.45 0.06	1.43 0.06	-0.0223	0.018	-0.1949	0.222
RD	0.57 0.04	0.59 0.03	0.0327	0.0113	0.4215	0.006
Cingulum*						
(L precuneus – R precuneus)						
FA	0.37 0.01	0.36 0.02	-0.0227	0.0082	-0.4025	0.0086
AD	1.18 0.05	1.18 0.05	-0.0128	0.018	-0.1117	0.4801
RD	0.65 0.03	0.67 0.04	0.0264	0.0131	0.3096	0.0503
Cingulum*						
(R inferior parietal cortex – superior parietal cortex)						
FA	0.44 0.03	0.42 0.03	-0.0163	0.0044	-0.5018	0.0005
AD	1.31 0.05	1.27 0.06	-0.0025	0.0158	-0.0246	0.8755
RD	0.61 0.03	0.63 0.03	0.019	0.0119	0.2443	0.1196
Cingulum*						
(R isthmuscingulate – posterior cingulate cortex)						
FA	0.42 0.02	0.40 0.02	-0.0249	0.0083	-0.4326	0.0045
AD	1.27 0.04	1.27 0.05	-0.0302	0.0177	-0.2614	0.095
RD	0.63 0.03	0.66 0.03	0.0174	0.0094	0.2863	0.0707
Cingulum*						
(R posterior cingulate cortex – precuneus)						
FA	0.52 0.02	0.50 0.03	-0.0184	0.0057	-0.4623	0.0024
AD	1.42 0.04	1.41 0.06	0.0064	0.0137	0.0741	0.6435
RD	0.57 0.04	0.59 0.04	0.0304	0.0096	0.4567	0.0029
Visual (lingual gyrus) network						
	HEU μ σ	HUU μ σ	β	std error	std β	p value
Forceps Major*						
(L cuneus – precuneus)						
FA	0.40 0.02	0.38 0.02	-0.0243	0.0064	-0.5045	0.0004
AD	1.23	1.21	-0.0177	0.0196	-0.1439	0.3697

	0.05 0.63	0.07 0.65				
RD	0.04	0.04	0.0222	0.0128	0.2558	0.0894
Forceps Major*						
(L cuneus – isthmuscingulate cortex)						
FA	0.41 0.02	0.40 0.03	-0.0218	0.0073	-0.4073	0.0047
AD	1.27 0.05	1.26 0.06	-0.0091	0.0189	-0.0776	0.6318
RD	0.64 0.04	0.66 0.04	0.0234	0.0122	0.2791	0.0608
Forceps Major						
(L lateral occipital cortex – superior parietal cortex)						
FA	0.38 0.03	0.36 0.02	-0.0254	0.0082	-0.4379	0.0037
AD	1.15 0.05	1.13 0.06	-0.0208	0.017	-0.1919	0.2297
RD	0.63 0.04	0.64 0.04	0.0187	0.0128	0.2246	0.151
Forceps Major						
(L lateral occipital cortex – pericalcarine)						
FA	0.40 0.02	0.38 0.02	-0.0218	0.0077	-0.417	0.0071
AD	1.24 0.06	1.23 0.08	0.0014	0.0219	0.0097	0.9503
RD	0.65 0.04	0.67 0.06	0.025	0.0161	0.2367	0.1291
Visual (occipital lobe) network						
	HEU μ σ	HUU μ σ	β	std error	std β	p value
Forceps Major*						
(L lateral occipital cortex – pericalcarine)						
FA	0.36 0.03	0.34 0.02	-0.0215	0.0068	-0.4379	0.003
AD	1.16 0.06	1.14 0.07	-0.018	0.0205	-0.1368	0.3843
RD	0.65 0.03	0.66 0.03	0.0115	0.0105	0.1699	0.2784
Forceps Major*						
(L lateral occipital cortex – superior parietal cortex)						
FA	0.40 0.03	0.37 0.02	-0.0254	0.0079	-0.46	0.0023
AD	1.16 0.05	1.15 0.05	-0.0164	0.0153	-0.1704	0.2892
RD	0.61 0.04	0.63 0.04	0.0222	0.0115	0.2933	0.0602
Forceps Major*						

(R inferior parietal cortex – lateral occipital cortex)						
FA	0.37 0.02	0.35 0.01	-0.0166	0.0052	-0.4643	0.0025
AD	1.12 0.04	1.12 0.06	0.0005	0.0166	0.0049	0.9757
RD	0.62 0.03	0.64 0.04	0.0201	0.0112	0.2756	0.0802
Forceps Major*						
(R lateral occipital cortex – superior parietal cortex)						
FA	0.39 0.03	0.37 0.02	-0.0215	0.0078	-0.4062	0.009
AD	1.17 0.05	1.15 0.07	-0.017	0.0205	-0.1319	0.4107
RD	0.62 0.04	0.64 0.04	0.0209	0.0123	0.2588	0.0981
Salince network						
	HEU μ σ	HUU μ σ	β	std error	std β	p value
IFOF						
(L lateral orbitofrontal cortex – parstriangularis)						
FA	0.39 0.02	0.38 0.02	-0.0177	0.006	-0.4188	0.0037
AD	1.13 0.03	1.14 0.03	0.0074	0.0098	0.1189	0.4559
RD	0.62 0.03	0.64 0.03	0.0254	0.0085	0.4283	0.0054
IFOF						
(L parsopercularis – parstriangularis)						
FA	0.38 0.02	0.37 0.02	-0.0169	0.0058	-0.4398	0.0041
AD	1.11 0.03	1.11 0.04	-0.0012	0.0112	-0.0171	0.9152
RD	0.62 0.03	0.63 0.03	0.0214	0.0084	0.3806	0.0145
IFOF						
(L parsopercularis – precentral gyrus)						
FA	0.39 0.03	0.37 0.02	-0.025	0.0056	-0.4262	0.0047
AD	1.15 0.04	1.16 0.04	-0.0107	0.0121	0.087	0.4304
RD	0.63 0.03	0.65 0.03	0.0235	0.0096	0.3006	0.0078
IFOF						
(L lateral orbitofrontal cortex – parsopercularis)						
FA	0.39 0.02	0.37 0.02	-0.0173	0.0055	-0.4065	0.0065
AD	1.14	1.13	-0.0072	0.0124	-0.0933	0.5636

	0.04	0.04				
RD	0.62	0.64	0.0204	0.0085	0.3585	0.0212
	0.03	0.03				
IFOF						
(L parsoperclaris – insula)						
	0.39	0.38				
FA	0.01	0.02	-0.0151	0.0069	-0.3981	0.0086
	1.16	1.16				
AD	0.03	0.03	-0.004	0.0102	-0.0619	0.7004
	0.62	0.64				
RD	0.02	0.02	0.0183	0.0069	0.3923	0.012
IFOF						
(L parstriangularis – insula)						
	0.42	0.40				
FA	0.02	0.02	-0.0191	0.0084	-0.4319	0.0084
	1.19	1.18				
AD	0.04	0.04	-0.0078	0.0117	-0.1051	0.5117
	0.61	0.63				
RD	0.02	0.02	0.0207	0.0073	0.414	0.0071
Motor network						
	HEU	HUU				
	μ	μ	β	std error	std β	p value
	σ	σ				
SLF*						
(L putamen – postcentral gyrus)						
	0.41	0.40				
FA	0.02	0.02	-0.0189	0.0061	-0.4483	0.0034
	1.18	1.17				
AD	0.04	0.05	-0.0093	0.0138	-0.1074	0.506
	0.60	0.62				
RD	0.02	0.02	0.0214	0.0072	0.4353	0.0048
SLF*						
(L putamen – superior temporal cortex)						
	0.43	0.41				
FA	0.03	0.03	-0.0264	0.0086	-0.4467	0.0038
	1.23	1.22				
AD	0.05	0.06	-0.012	0.0171	-0.112	0.4877
	0.61	0.63				
RD	0.02	0.03	0.0242	0.0075	0.4657	0.0024
SLF*						
(L parsopercularis – precentral gyrus)						
	0.39	0.37				
FA	0.02	0.02	-0.0169	0.0053	-0.4571	0.0027
	1.16	1.16				
AD	0.03	0.03	0.005	0.0096	0.0808	0.6031
	0.63	0.66				
RD	0.03	0.03	0.025	0.0085	0.4244	0.0051
SLF*						

(L postcentral gyrus – insula)						
FA	0.40 0.02	0.38 0.02	-0.02	0.0059	-0.4792	0.0014
AD	1.16 0.04	1.15 0.04	-0.0079	0.0128	-0.0985	0.5423
RD	0.62 0.02	0.64 0.02	0.023	0.0076	0.4376	0.004
SLF*						
(L precentral gyrus – insula)						
FA	0.41 0.02	0.39 0.02	-0.0198	0.0065	-0.4368	0.0039
AD	1.18 0.04	1.19 0.05	-0.0028	0.0118	-0.0378	0.8142
RD	0.62 0.02	0.64 0.03	0.0226	0.0076	0.4231	0.005
SLF						
(L postcentral gyrus – precentral gyrus)						
FA	0.37 0.01	0.36 0.01	-0.0105	0.0039	-0.3983	0.0097
AD	1.15 0.03	1.16 0.04	0.0109	0.0105	0.1581	0.3077
RD	0.65 0.02	0.67 0.03	0.0202	0.0088	0.3428	0.0259

*survived FDR multiple comparisons correction $p < 0.05$. R = right; L = left.

5. DISCUSSION

As the brain develops, the conduction speed of nerve impulses increases with myelination and likely contributes to increases in functional connectivity (Paus, 2010; Salzer & Zalc, 2016). Given the interdependence of functional and structural networks in the brain, investigating the properties of WM tracts within functional networks provides a necessary link between HIV associated WM abnormalities and brain function. We examined the effects of HIV/ART on structural connectivity in the developing brain by looking at WM tracts connecting specific GM regions within functional networks in 7-year-old children. We find abnormalities associated with HIV infection and exposure across tracts within several networks. To our knowledge, this is the first study to examine structural connectivity within functional networks of HIV+ and HEU children.

Between 5 and 10 years, the developing the brain is undergoing significant functional and structural restructuring. Functional networks are in an intermediate developmental stage where intra-network connectivity is not as weak as it was in infancy but not yet as strong as it will be in adulthood (Power et al., 2010). WM tracts are maturing with improved oligodendrocyte proliferation, the glial cells responsible for the formation of myelin, which continues into late teen years and even early 20s for some structures. One DTI study shows that between the ages of 5 and 10, WM tracts undergo rapid increase in FA, a decrease in MD and then a steady maturation thereafter thus making this a vulnerable time for abnormalities (Lebel et al., 2008).

5.1 HIV+ vs CONTROLS

We present a discussion of the findings first focused on the implicated functional networks, followed by a summary of the specific WM connections involved.

Functional Networks

In our RS-fMRI study at 7 years, we found reduced connectivity within the DMN. We also found higher RS connectivity to be related to measures of reduced immune health (CD4 and CD4%) in infancy in the basal ganglia, somatosensory and salience networks. Given the alterations in these networks related to HIV infection, we posited that WM tracts within these specific networks would likely also be affected. Our

analysis did indeed identify WM tracts associated with four specific networks. While there is some overlap in the GM regions with HIV-associated functional changes, not all of the seeds and clusters previously reported show up in this analysis. This may be due to the smaller sample size in the functional study (45 subjects) compared to this analysis (107 subjects), which was caused by lack of RS-fMRI acquired at age 7. It may also reflect indirect WM pathways involved in functional networks.

In addition, we also identified WM connections affected by HIV infection within the motor and auditory networks. We had hypothesized possible HIV-related alterations in both networks based on clusters identified in our voxelwise DTI analysis at 7 years.

After adjusting for multiple comparisons, most of the connections identified were no longer statistically significant at the $p<0.05$ level except for those in the DMN, salience and somatosensory network.

DMN. This network shows BOLD activity when an individual is not executing any task/daydreaming active during rest and is involved in episodic memory processing, consists primarily of the posterior cingulate cortex, medial temporal lobe and the medial prefrontal cortex. The DMN showed decreased intra-network functional connectivity using seed based functional connectivity analysis in HIV+ children in this cohort at age 7 (Toich et al., 2018) and another cohort of perinatally infected youth (Herting et al., 2015). In this analysis, we find altered structural connectivity (higher MD) in HIV+ children. Notably in both the functional analysis and the current structural analysis, the medial frontal cortex was involved which suggests that the effects of HIV infection in this region have both functional and structural consequences. Previous work has shown that associations between functional and structural connectivity, including in the DMN, where FA of the cingulum bundle was associated with partial correlations of BOLD signals from GM regions connected by this tract (van den Heuvel et al., 2008). In our work, we find altrations in the FM which may alter DMN connectivity due to the interconnectedness of structure and function.

Salience network. The salience network had the highest number of affected WM tracts. This is a higher order cognitive network that undergoes significant maturation during early adolescence. This network is comprised primarily of the anterior insula and dorsal anterior cingulate cortex and manages neural responses to external sensory information (Seeley et al., 2007). In terms of number of structural connections,

it is the biggest functional network, having four times the amount of connections in the smallest functional network, the DMN. The salience network has been shown to demonstrate lower intranetwork connectivity in HIV+ adults despite viral load suppression (Chaganti et al., 2017) but not in children. Although we didn't find altered connectivity within the salience network, we found both higher and lower connectivity between it and other networks in HIV+ children (Toich et al., 2018) demonstrating that this network is quite vulnerable to HIV. And, we found connectivity within the salience network (R inferior frontal gyrus and insula) to be associated with immune health markers (CD4%) in infancy (Toich et al., 2018). However, this cluster does not overlap with any of the GM regions found to have altered WM connections. This could be due to the larger sample size in the current analysis. Both functional and structural analyses within this cohort implicate the salience network and WM connections within; all these results point to a particular vulnerability to HIV related developmental delays in this network even in the presence of early ART initiation.

Somatosensory network. As with the salience network, previous functional analysis in a smaller group of children found associations between functional connectivity in the somatosensory network and immune health markers (CD4%) in infancy. Similar to the results in the salience network, there isn't a correspondence between the GM regions which is likely due to low statistical power in the RS-fMRI study. We find the superior frontal cortex repeatedly amongst the GM regions showing HIV related changes. The connection between the superior frontal cortex and posterior cingulate cortex is seen in both hemispheres. These point to specific HIV related regional susceptibilities within this network to the effects in the developing brain.

White matter tracts

The observed WM abnormalities in FA and MD were largely attributable to increases in RD in HIV+ children. In healthy subjects, RD declines significantly with age whereas AD undergoes very little to no change with age (Lebel et al., 2008). Thus, because of the changes that perpendicular diffusivity is undergoing, any effect of HIV/ART can alter the growth trajectory. From this we also learn that the WM deficits perceived are most likely due to complications in myelination or axonal packing. Since myelination proceeds throughout childhood and adolescents, the WM alterations perceived in the HIV+ children here could be due to delays in WM maturation. However, since RD can

also be an indication of axonal packing or bundle thickness, we can not rule out altered axonal packing as an explanation for these results. Future work may also focus on investigating number of streamlines as a function of the different groups as this may give more clarity on understanding these WM alterations.

We observe different regions of the IFOF consistently showing damage in previous voxelwise studies at age 5 and 7 (Ackermann et al., 2016; Jankiewicz et al., 2017). In the voxelwise DTI study we observed both the ATR and FM (Jankiewicz et al., 2017) which we also found to be affected in the current study. The ATR is implicated in the salience network mostly as well as the DMN, while the FM is implicated in the DMN. This not only points to the vulnerability of these tracts, but also the specific functional networks that could be potentially affected by alterations to these tracts during development. Furthermore, we did not find the superior corona radiata as well as the ILF, both of which have been implicated in the previous voxelwise DTI study. This may be due to the fact that the current study was restricted to tractography within the boundaries of the specific functional networks whereas the voxelwise DTI study was a whole brain analysis.

The cingulum, SLF, forceps minor and ATR seem to be the most heavily affected WM tracts, each being implicated multiple times in at least two functional networks. We can broadly divide WM tracts into three groups: association fibres which connect two cortical regions within the same hemisphere, projection fibres which connect cortical regions to subcortical regions and commissural fibres which connect GM regions of the left hemisphere with those of the right (Mori et al., 2005). The cingulum and SLF are both long association fibres, the ATR is a projection fibre and the forceps minor is a commissural fibre. Though commissural fibres generally have higher anisotropy than projection fibres which in turn have higher anisotropy than association fibres (Mori & Zhang, 2006) it seems all three are affected the same suggesting that HIV does not have specific WM targets.

The affected WM connections seem to be mostly from superior frontal cortex regions, putamen and insula. Both (Toich et al., 2018) and (Herting et al., 2015) found the frontal cortical regions to be the most affected which shows that the frontal cortex is at particular risk both in structure and function. Deep GM structures such as the putamen, which is part of the basal ganglia, mature throughout childhood. Through childhood

and adolescence, the WM fibres connecting the regions become better organized i.e. increased myelination and/or improved axonal packing (Lebel et al., 2008) and there is also a decrease in total GM volume. The early influences of HIV/ART can alter the course of these developing structures.

5.2 HEU vs HUU

We observed higher FA in HEU children compared to HUU children within tracts in the pDMN, visual (occipital lobe and lingual gyrus), salience and motor networks. Consistent with the voxelwise DTI study, the current found higher FA in affected, however, neither the posterior corona radiata nor the CST, were present in the current study. Again, possibly because the current analysis was not a whole brain analysis as was the case in the voxelwise DTI analysis. Furthermore, results from the functional connectivity analysis on HEU vs HUU, which can be found in a thesis write-up by Toich *et al,* showed increased functional connectivity in clusters within the DMN, pDMN, executive and motor networks in HEU children compared to HUU. Though the sample size was small (n=8 HEU, n=10 HUU) compared to the size of the current study, these results suggest that altered functional connectivity due to HIV exposure may be related to altered functional connectivity in pDMN and motor network.

Further, we see the cingulum, IFOF and SLF being affected, as in the HIV+ vs controls analyses, but now in different networks suggesting that these WM tracts are the most vulnerable to HIV/ART effects. Higher FA values in the HEU children are counterintuitive but these results are consistent with the previous voxelwise DTI study which found higher FA values in HEU children in a region of the superior corona radiata (Jankiewicz et al., 2017) and in middle cerebellar peduncles of HEU neonates (Tran et al., 2016). FA as an indicator of axonal integrity is a measure of axonal diameter, axonal pocking density and axonal branching (Hoeft et al., 2007). An alteration in any of these will lead to either an increase or decrease in FA. This, together with the understanding that FA increases at a certain rate over a certain time, means that premature increases in FA are as much abnormal as delayed increases. We found no significant group differences in MD, which suggests that HIV exposure affects the axons directly.

With all the results, the left hemisphere seems to be more affected than the right. There have been studies that have shown that the SLF and cingulum bundle have higher anisotropy values in the left than in the right hemisphere (Lebel et al., 2008). If the tracts in the left hemisphere develop better and faster than the right, this could explain why they are affected more than the right.

6. CONCLUSIONS

In conclusion, as hypothesised we found altered structural connectivity in the somatosensory, auditory, salience, default mode, motor and basal ganglia networks of HIV+ children compared to uninfected controls. The basal ganglia, default mode, salience and somatosensory networks have all been found to have altered functional connectivity in a previous study which suggests that damage or developmental delay in WM may be related to or responsible for the HIV-associated functional abnormalities. Both FA and MD differences were largely attributable to RD increases suggesting demyelination/dysmyelination due to HIV/ART.

In addition, we examined the effects of HIV exposure and found increased structural connectivity, in the visual networks, pDMN, salience and motor network. Higher FA is consistent with the previous voxelwise DTI study performed on the same cohort and suggest that HIV/ART exposure may result in premature axonal maturation in the developing brain.

7. Limitations

A limitation of the current study is that we did not do correlation analyses between the functional and structural connectivity as this would show whether the alterations we see in both are in fact related. Furthermore, it would have been helpful to examine the association between disease severity and structural connectivity to perform a more complete comparison between functional and structural connectivity results. Future work could focus on these associations as well a whole brain tractography analysis.

REFERENCES

Ackermann, C, Andronikou, S., Saleh, M. G., Laughton, B., Alhamud, A. A., van der Kouwe, A., … Meintjes, E. M. (2016). Early Antiretroviral Therapy in HIV-Infected Children Is Associated with Diffuse White Matter Structural Abnormality and Corpus Callosum Sparing. *AJNR. American Journal of Neuroradiology*, 2363–2369. https://doi.org/10.3174/ajnr.A4921

Ackermann, Christelle, Andronikou, S., Saleh, M. G., Laughton, B., Alhamud, A. A., Van Der Kouwe, A., … Meintjes, E. M. (2016). Early antiretroviral therapy in HIV-infected children is associated with diffuse white matter structural abnormality and corpus callosum sparing HHS Public Access. *AJNR Am J Neuroradiol*, *37*(12), 2363–2369. https://doi.org/10.3174/ajnr.A4921

AFNI. (2014). AFNI program: 3dNwarpApply. Retrieved December 24, 2018, from https://afni.nimh.nih.gov/pub/dist/doc/program_help/3dNwarpApply.html

Alexander, A. L., Hurley, S. A., Samsonov, A. A., Adluru, N., Hosseinbor, A. P., Mossahebi, P., … Field, A. S. (2011). Characterization of Cerebral White Matter Properties Using Quantitative Magnetic Resonance Imaging Stains. *Brain Connectivity*, *1*(6), 423–446. https://doi.org/10.1089/brain.2011.0071

Alhamud, A., Tisdall, M. D., Hess, A. T., Hasan, K. M., Meintjes, E. M., & Van Der Kouwe, A. J. W. (2012). Volumetric navigators for real-time motion correction in diffusion tensor imaging. *Magnetic Resonance in Medicine*, *68*(4), 1097–1108. https://doi.org/10.1002/mrm.23314

Ann, H. W., Jun, S., Shin, N. Y., Han, S., Ahn, J. Y., Ahn, M. Y., … Choi, J. Y. (2016). Characteristics of resting-state functional connectivity in HIV-associated neurocognitive disorder. *PLoS ONE*, *11*(4), 1–11. https://doi.org/10.1371/journal.pone.0153493

Arts, E. J., & Hazuda, D. J. (2012). HIV-1 antiretroviral drug therapy. *Cold Spring Harbor Perspectives in Medicine*, *2*(4). https://doi.org/10.1101/cshperspect.a007161

Attia, S., Egger, M., Müller, M., Zwahlen, M., & Low, N. (2009). Sexual transmission of HIV according to viral load and antiretroviral therapy: Systematic review and meta-analysis. *Aids*, *23*(11), 1397–1404. https://doi.org/10.1097/QAD.0b013e32832b7dca

Basser, P. J., & Pierpaoli, C. (1996). Microstructural and physiological features of tissues elucidated by quantitative-diffusion-tensor MRI. *Journal of Magnetic Resonance - Series B*, *111*(3), 209–219. https://doi.org/10.1006/jmrb.1996.0086

Benjamini, Y., & Hochberg, Y. (1995). Controlling the False Discovery Rate : A Practical and Powerful Approach to Multiple Testing Author (s): Yoav Benjamini and Yosef Hochberg Source : Journal of the Royal Statistical Society . Series B (Methodological), Vol . 57 , No . 1 Published by : *J. R. Statist. Soc.*, *57*(1), 289–300.

Berger, P. B. (1996). [science in medicine * science medicale I HOPE AND CAUTION: REPORT

FROM THE XL INTERNATIONAL CONFERENCE ON AIDS Infornation provided at the conference represented the result of over a decade's worth of study on the pathogenesis of HIV infection and on th, *155*(6), 717–721. Retrieved from https://www.ncbi.nlm.nih.gov/pmc/articles/PMC1335225/pdf/cmaj00102-0107.pdf

Boissé, L., Gill, M. J., & Power, C. (2008). HIV Infection of the Central Nervous System: Clinical Features and Neuropathogenesis. *Neurologic Clinics*, *26*(3), 799–819. https://doi.org/10.1016/j.ncl.2008.04.002

Carvalhal, A., Gill, M. J., Letendre, S. L., Rachlis, A., Bekele, T., Raboud, J., … Rourke, S. B. (2016). Central nervous system penetration effectiveness of antiretroviral drugs and neuropsychological impairment in the Ontario HIV Treatment Network Cohort Study. *Journal of NeuroVirology*, 349–357. https://doi.org/10.1007/s13365-015-0404-5

CDC. (2017). Pregnant Women, Infants, and Children | Gender | HIV by Group | HIV/AIDS | CDC. Retrieved September 25, 2018, from https://www.cdc.gov/hiv/group/gender/pregnantwomen/index.html

Chaganti, X. J. R., Heinecke, X. A., Gates, X. T. M., Moffat, X. K. J., & Brew, X. B. J. (2017). Functional Connectivity in Virally Suppressed Patients with HIV-Associated Neurocognitive Disorder : A Resting-State Analysis, 1–7.

Chen, Z., Ni, P., Zhang, J., Ye, Y., Xiao, H., Qian, G., … Zeng, Y. (2008). Evaluating ischemic stroke with diffusion tensor imaging. *Neurological Research*, *30*(7), 720–726. https://doi.org/10.1179/174313208X297968

Cotton, M., Violari, A., Otwombe, K., Panchia, R., Dobbels, E., Rabie, H., … AG., B. (2014). Early limited antiretroviral therapy is superior to deferred therapy in HIV-infected South African infants: results from the CHER (Children with HIV Early antiRetroviral) Randomized Trial Mark, *382*(9904), 1555–1563. https://doi.org/10.1016/S0140-6736(13)61409-9.Early

Cox, R. W. (1996). AFNI: software for analysis and visualization of functional magnetic resonance neuroimages. *Computers and Biomedical Research, an International Journal*, *29*(3), 162–173. https://doi.org/10.1006/cbmr.1996.0014

Descoteaux, M., Deriche, R., Anwander, A., Anw, A., Bio, T. T., Odyssée, P., & Odyss��e, P. (2007). Deterministic and probabilistic q-ball tractography: from diffusion to sharp fiber distributions, (August), 36. https://doi.org/10.1016/j.mcn.2008.05.017

Dietrich, O., Biffar, A., Baur-Melnyk, A., & Reiser, M. F. (2010). Technical aspects of MR diffusion imaging of the body. *European Journal of Radiology*, *76*(3), 314–322. https://doi.org/10.1016/j.ejrad.2010.02.018

Dua, H. S., & Singh, A. D. (2010). *MRI At a glance*. *British Journal of Ophthalmology* (Vol. 94).

https://doi.org/10.1136/bjo.2010.193169

Eisfeld, C., Reichelt, D., & Evers, S. (2013). CSF Penetration by Antiretroviral Drugs, 31–55. https://doi.org/10.1007/s40263-012-0018-x

Ellis, R. J., Calero, P., & Stockin, M. D. (2009). HIV infection and the central nervous system: A primer. *Neuropsychology Review*, *19*(2), 144–151. https://doi.org/10.1007/s11065-009-9094-1

Ene, L., Duiculescu, D., & Ruta, S. M. (2011). How much do antiretroviral drugs penetrate into the central nervous system? *Journal of Medicine and Life*, *4*(4), 432–439. https://doi.org/10.1007/s40262-015-0257-3

Feldman, H., J. Yeatman, E. Lee, L. B., & Gaman-Bean, S. (2010). Diffusion Tensor Imaging: A Review for Pediatric Researchers and Clinicians, *31*(4), 346–356. https://doi.org/10.1097/DBP.0b013e3181dcaa8b.Diffusion

Ghosh, N., Holshouser, B., Oyoyo, U., Barnes, S., Tong, K., & Ashwal, S. (2017). Combined Diffusion Tensor and Magnetic Resonance Spectroscopic Imaging Methodology for Automated Regional Brain Analysis: Application in a Normal Pediatric Population. *Developmental Neuroscience*, *39*(5), 413–429. https://doi.org/10.1159/000475545

Gnanakaran, S., Lang, D., Daniels, M., Bhattacharya, T., Derdeyn, C. A., & Korber, B. (2007). Clade-specific differences between human immunodeficiency virus type 1 clades B and C: diversity and correlations in C3-V4 regions of gp120. *Journal of Virology*, *81*(9), 4886–4891. https://doi.org/10.1128/JVI.01954-06

Greicius, M. D., Supekar, K., Menon, V., & Dougherty, R. F. (2009). Resting-state functional connectivity reflects structural connectivity in the default mode network. *Cerebral Cortex*, *19*(1), 72–78. https://doi.org/10.1093/cercor/bhn059

Hagmann, P, Jonasson, L., Maeder, P., Thiran, J. P., Wedeen, V. J., & Meuli, R. (2006). Understanding diffusion MR imaging techniques: from scalar diffusion-weighted imaging to diffusion tensor imaging and beyond. *Radiographics*, *26 Suppl 1*, S205-23. https://doi.org/10.1148/rg.26si065510

Hagmann, Patric, Cammoun, L., Gigandet, X., Meuli, R., Honey, C. J., Van Wedeen, J., & Sporns, O. (2008). Mapping the structural core of human cerebral cortex. *PLoS Biology*, *6*(7), 1479–1493. https://doi.org/10.1371/journal.pbio.0060159

Herting, M. M., Uban, K. A., Williams, P. L., Gautam, P., Huo, Y., Malee, K., … Sowell, E. R. (2015). Default Mode Connectivity in Youth With Perinatally Acquired HIV. *Medicine*, *94*(37), e1417. https://doi.org/10.1097/MD.0000000000001417

HIV.gov. (2018). Global Statistics | HIV.gov. Retrieved November 18, 2018, from https://www.hiv.gov/hiv-basics/overview/data-and-trends/global-statistics

Hoare, J., Fouche, J.-P., Phillips, N., Joska, J. A., Paul, R., Donald, K. A., … Stein, D. J. (2015). White matter micro-structural changes in ART-naive and ART-treated children and adolescents infected with HIV in South Africa. *Aids*, *29*(14), 1793–1801. https://doi.org/10.1097/QAD.0000000000000766

Hoare, J., Fouche, J. P., Phillips, N., Joska, J. A., Donald, K. A., Thomas, K., & Stein, D. J. (2015). Clinical associations of white matter damage in cART-treated HIV-positive children in South Africa. *Journal of NeuroVirology*, *21*(2), 120–128. https://doi.org/10.1007/s13365-014-0311-1

Hoare, J., Fouche, J. P., Spottiswoode, B., Donald, K., Philipps, N., Bezuidenhout, H., … Stein, D. (2012). A diffusion tensor imaging and neurocognitive study of HIV-positive children who are HAART-naïve "slow progressors." *Journal of NeuroVirology*, *18*(3), 205–212. https://doi.org/10.1007/s13365-012-0099-9

Hoeft, F., Barnea-Goraly, N., Haas, B. W., Golarai, G., Ng, D., Mills, D., … Reiss, A. L. (2007). More Is Not Always Better: Increased Fractional Anisotropy of Superior Longitudinal Fasciculus Associated with Poor Visuospatial Abilities in Williams Syndrome. *Journal of Neuroscience*, *27*(44), 11960–11965. https://doi.org/10.1523/JNEUROSCI.3591-07.2007

Honey, C. J., Honey, C. J., Sporns, O., Sporns, O., Cammoun, L., Cammoun, L., … Hagmann, P. (2009). Predicting human resting-state functional connectivity from structural connectivity. *Proceedings of the National Academy of Sciences of the United States of America*, *106*(6), 2035–2040. https://doi.org/10.1073/pnas.0811168106

Hua, K., Zhang, J., Wakana, S., Jiang, H., Li, X., Reich, D. S., … Mori, S. (2008). Tract probability maps in stereotaxic spaces: analyses of white matter anatomy and tract-specific quantification. *NeuroImage*, *39*(1), 336–347. https://doi.org/10.1016/j.neuroimage.2007.07.053

Jankiewicz, M., Holmes, M. J., Taylor, P. A., Cotton, M. F., Laughton, B., van der Kouwe, A. J. W., & Meintjes, E. M. (2017). White Matter Abnormalities in Children with HIV Infection and Exposure. *Frontiers in Neuroanatomy*, *11*(September), 1–9. https://doi.org/10.3389/fnana.2017.00088

Koch, M. A., Norris, D. G., & Hund-Georgiadis, M. (2002). An investigation of functional and anatomical connectivity using magnetic resonance imaging. *NeuroImage*, *16*(1), 241–250. https://doi.org/10.1006/nimg.2001.1052

Kumar, A. (2014). History of MRI. *Journal of the Indian Institute of Science*, *94*(4), 363–370.

Lebel, C., Walker, L., Leemans, A., Phillips, L., & Beaulieu, C. (2008). Microstructural maturation of the human brain from childhood to adulthood. *NeuroImage*, *40*(3), 1044–1055. https://doi.org/10.1016/j.neuroimage.2007.12.053

Letendre, S., Marquie-beck, J., Capparelli, E., Best, B., Clifford, D., Collier, A. C., … Group, C. (2009). Validation of the CNS Penetration-Effectiveness Rank for Quantifying Antiretroviral Penetration

Into the Central Nervous System, *65*(1), 65–70. https://doi.org/10.1001/archneurol.2007.31.Validation

Li, X. J., Wu, G., Wen, Z., Zhang, J., Lei, H., Gui, X., & Lin, X. F. (2015). White Matter Development is Potentially Influenced in Adolescents with Vertically Transmitted HIV Infections : A Tract-Based Spatial Statistics Study, 1–7.

Maartens, G., Celum, C., & Lewin, S. R. (2014). HIV infection: Epidemiology, pathogenesis, treatment, and prevention. *The Lancet*, *384*(9939), 258–271. https://doi.org/10.1016/S0140-6736(14)60164-1

Madhi, S. A., Adrian, P., Cotton, M. F., McIntyre, J. A., Jean-Philippe, P., Meadows, S., … Violari, A. (2010). Effect of HIV Infection Status and Anti-Retroviral Treatment on Quantitative and Qualitative Antibody Responses to Pneumococcal Conjugate Vaccine in Infants. *The Journal of Infectious Diseases*, *202*(3), 355–361. https://doi.org/10.1086/653704

Molfese, P., Glen, D., Mesite, L., Pugh, K., & Cox, R. (2011). The Haskins Pediatric Brain Atlas, *8*, 8.

Mori, S., & Zhang, J. (2006). Principles of Diffusion Tensor Imaging and Its Applications to Basic Neuroscience Research. *Neuron*, *51*(5), 527–539. https://doi.org/10.1016/j.neuron.2006.08.012

Ni, H., Kavcic, V., Zhu, T., Ekholm, S., & Zhong, J. (2006). Effects of number of diffusion gradient directions on derived diffusion tensor imaging indices in human brain. *AJNR. American Journal of Neuroradiology*, *27*(8), 1776–1781. Retrieved from http://www.ncbi.nlm.nih.gov/pubmed/16971635

O'Donnell, L. J., & Westin, C.-F. (2011a). An Introduction to Diffusion Tensor Image Analysis. *Neurosurgery Clinics of North America*, *22*(2), 185–196. https://doi.org/10.1016/j.nec.2010.12.004

O'Donnell, L. J., & Westin, C. F. (2011b). An introduction to diffusion tensor image analysis. *Neurosurgery Clinics of North America*, *22*(2), 185–196. https://doi.org/10.1016/j.nec.2010.12.004

Ortega, M., Brier, M. R., & Ances, B. M. (2015). Effects of HIV and combination antiretroviral therapy on cortico-striatal functional connectivity, (January). https://doi.org/10.1097/QAD.0000000000000611

Paus, T. (2010). Growth of white matter in the adolescent brain: Myelin or axon? *Brain and Cognition*, *72*(1), 26–35. https://doi.org/10.1016/j.bandc.2009.06.002

Pfefferbaum, A., Adalsteinsson, E., Rohlfing, T., & Sullivan, E. V. (2010). Diffusion tensor imaging of deep gray matter brain structures: effects of age and iron concentration. *Neurobiology of Aging*, *31*(3), 482–493. https://doi.org/10.1016/j.neurobiolaging.2008.04.013

Pierpaoli, C., Walker, L., Irfanogula, M., Barnett, A., Basser, P., Chang, L., … M, W. (2009). TORTOISE: an integrated software package for processing of diffusion MRI data, *51*(1), 2009.

Power, J., Fair, D., Schlaggar, B., & Petersen, S. (2010). The development of Human Functional Brain Networks. *Neuron*, *67*(5), 735–748. https://doi.org/10.1016/j.neuron.2010.08.017.The

Rulseh, A. M., Keller, J., Tintěra, J., Kožíšek, M., & Vymazal, J. (2013). Chasing shadows: What determines DTI metrics in gray matter regions? An in vitro and in vivo study. *Journal of Magnetic Resonance Imaging*, *38*(5), 1103–1110. https://doi.org/10.1002/jmri.24065

Salzer, J. L., & Zalc, B. (2016). Myelination. *Current Biology*, *26*(20), R971–R975. https://doi.org/10.1016/j.cub.2016.07.074

Sbardella, E., Tona, F., Petsas, N., & Pantano, P. (2013). DTI Measurements in Multiple Sclerosis: Evaluation of Brain Damage and Clinical Implications. *Multiple Sclerosis International*, *2013*, 1–11. https://doi.org/10.1155/2013/671730

Seeley, W. W., Menon, V., Schatzberg, A. F., Keller, J., Gary, H., Kenna, H., … Greicius, M. D. (2007). Dissociable Intrinsic Connectivity Networks for Salience Processing and Executive Control. *J Neurosci*, *27*(9), 2349–2356. https://doi.org/10.1523/JNEUROSCI.5587-06.2007.Dissociable

Shah, A., Gangwani, M. R., Chaudhari, N. S., & Glazyrin, A. (2016). Neurotoxicity in the Post-HAART Era : Caution for the Antiretroviral Therapeutics. *Neurotoxicity Research*, *30*(4), 677–697. https://doi.org/10.1007/s12640-016-9646-0

Skudlarski, P., Jagannathan, K., Calhoun, V. D., Hampson, M., Skudlarska, B. A., & Pearlson, G. (2008). Measuring brain connectivity: Diffusion tensor imaging validates resting state temporal correlations. *NeuroImage*, *43*(3), 554–561. https://doi.org/10.1016/j.neuroimage.2008.07.063

StatsSA. (2018). Statistical release- Mid-year population estimates July 2018. *Africa*, (P0302, July), 1–22. https://doi.org/Statistical release P0302

Streck, E. L., Scaini, G., & Rezin, G. T. (2008). Effects of the HIV treatment drugs nevirapine and efavirenz on brain creatine kinase activity, 485–492. https://doi.org/10.1007/s11011-008-9109-2

Susumu Mori, S. Wakana, Peter C M van Zijl, L. M. N.-P. (2005). *MRI Atlas of Human White Matter*. Retrieved from https://books.google.co.za/books?hl=en&lr=&id=ltwRYlvFNLIC&oi=fnd&pg=PR5&dq=mri+atlas+of+human+white+matter&ots=gdJIl92Plp&sig=PY6S9OPkNcGVOlBQTmQXsMGwGNU#v=onepage&q=mri atlas of human white matter&f=false

Taylor, P. a, & Saad, Z. S. (2013). FATCAT: (An Efficient) Functional And Tractographic Connectivity Analysis Toolbox. *Brain Connectivity*, *3*(5), 523–535. https://doi.org/10.1089/brain.2013.0154

Taylor, P., Chen, G., Cox, R., & Saad, Z. (2015). Open Environment for Multimodal Interactive Connectivity Visualization and Analysis. *Brain Connectivity*, *XX*(Xx), 36. https://doi.org/10.1016/j.mcn.2008.05.017

Thomas, J. B., Brier, M. R., Snyder, A. Z., Vaida, F. F., & Ances, B. M. (2013). Pathways to neurodegeneration: Effects of HIV and aging on resting-state functional connectivity. *Neurology*, *80*(13). https://doi.org/10.1212/WNL.0b013e318288792b

Toich, J. T. F., Taylor, P. A., Holmes, M. J., Gohel, S., Cotton, M. F., Dobbels, E., … Meintjes, E. M. (2018). Functional Connectivity Alterations between Networks and Associations with Infant Immune Health within Networks in HIV Infected Children on Early Treatment: A Study at 7 Years. *Frontiers in Human Neuroscience*, *11*(January), 1–15. https://doi.org/10.3389/fnhum.2017.00635

Tran, L. T., Roos, A., Fouche, J.-P., Koen, N., Woods, R. P., Zar, H. J., … Donald, K. A. (2016). White Matter Microstructural Integrity and Neurobehavioral Outcome of HIV-Exposed Uninfected Neonates. *Medicine*, *95*(4), e2577. https://doi.org/10.1097/MD.0000000000002577

Tromp, D. (2016). DTI Scalars (FA, MD, AD, RD) - How do they relate to brain structure? *The Winnower*. https://doi.org/10.15200/WINN.146119.94778

Uban, K., Herting, M., Williams, P., Tanvi, A., Gautam, P., Yanling, H., & Nichols, S. et al. (2016). White matter microstructure among youth with perinatally acquired HIV is associated with disease severity, *93*(4), 292–297. https://doi.org/10.1016/j.contraception.2015.12.017.Women

UNAIDS. (2018). UNAIDS Global statistics 2018, (July), 1–5. Retrieved from http://www.unaids.org/sites/default/files/media_asset/UNAIDS_FactSheet_en.pdf

van den Heuvel, M., Mandl, R., Luigjes, J., & Hulshoff Pol, H. (2008). Microstructural Organization of the Cingulum Tract and the Level of Default Mode Functional Connectivity. *Journal of Neuroscience*, *28*(43), 10844–10851. https://doi.org/10.1523/JNEUROSCI.2964-08.2008

Van Rie, A., Harrington, P. R., Dow, A., & Robertson, K. (2007). Neurologic and neurodevelopmental manifestations of pediatric HIV/AIDS: A global perspective. *European Journal of Paediatric Neurology*, *11*(1), 1–9. https://doi.org/10.1016/j.ejpn.2006.10.006

Wakana, S., Caprihan, A., Panzenboeck, M. M., Fallon, J. H., Perry, M., Gollub, R. L., … Mori, S. (2007). Reproducibility of quantitative tractography methods applied to cerebral white matter. *NeuroImage*, *36*(3), 630–644. https://doi.org/10.1016/j.neuroimage.2007.02.049

Wang, X., Foryt, P., Ochs, R., Chung, J.-H., Wu, Y., Parrish, T., & Ragin, A. B. (2011). Abnormalities in Resting-State Functional Connectivity in Early Human Immunodeficiency Virus Infection. *Brain Connectivity*, *1*(3), 207–217. https://doi.org/10.1089/brain.2011.0016